Discover Materials

https://doi.org/10.1007/s43939-026-00845-7

Article in Press

A peptide library approach to biofunctionalized electrospun PLGA scaffolds for tunable endothelial cell responses

Received: 16 April 2026

Accepted: 16 July 2026

Published online: 21 July 2026

Cite this article as: Erdogan N., Chiesa E., Rosalia M. *et al.* A peptide library approach to biofunctionalized electrospun PLGA scaffolds for tunable endothelial cell responses. *Discov Mater* (2026). https://doi.org/10.1007/s43939-026-00845-7

Nursu Erdogan, Enrica Chiesa, Mariella Rosalia, Dhriti Santosh Shenoy, Kaliroi Peqini, Sara Pellegrino & Ida Genta

A Peptide Library Approach to Biofunctionalized Electrospun PLGA Scaffolds for Tunable Endothelial Cell Responses

Nursu Erdogan[1,2,3], Enrica Chiesa[1,*], Mariella Rosalia[1], Dhriti Santosh Shenoy[4], Kaliroi Peqini[4], Sara Pellegrino[4], Ida Genta[1,*]

[1] Department of Drug Sciences, Pharmaceutical Technology and Law Laboratory, University of Pavia, Viale Torquato Taramelli 12, Pavia, Italy

[2] Physics of Nanostructures and Advanced Materials, University of the Basque Country, Barrio Sarriena s/n, Leioa, Bizkaia, Spain

[3]CIC nanoGUNE BRTA, Tolosa Hiribidea, 76, Donostia-San Sebastian, Spain

[4]DISFARM, Department of Pharmaceutical Sciences, Section of General and Organic Chemistry, A. Marchesini, University of Milan, Milan, Italy

*Corresponding authors

E-mail address: *ida.genta@unipv.it; *enrica.chiesa@unipv.it

ABSTRACT:

Engineering the biomaterial interface is the critical step for directing cell behavior and improving the performance of tissue-engineered scaffolds. This study aimed to establish a systematic interface engineering strategy by functionalizing electrospun scaffolds with a library of peptide motifs and evaluating their biocompatibility as well as dose effects on early cellular responses. Electrospun poly(lactide-co-glycolide) (PLGA) scaffolds with randomly oriented fibers were produced, taking advantage of PLGA's biocompatibility, mechanical integrity, and reactive end groups that enable surface functionalization. Five cysteine-modified peptides (IKVAV, REDV, GFOGER, (D-Phe)PRP, and KAFDITYVRLKF) were synthesized at high purity and conjugated to maleimide-activated PLGA using thiol coupling. Peptide-enriched scaffolds were systematically assessed and compared for conjugation efficiency, physicochemical and surface properties, cytotoxicity, and biocompatibility in both fibroblast and endothelial cells. Peptide conjugation preserved scaffold morphology and did not measurably affect bulk properties. Cytotoxicity assays indicated that KAFDITYVRLKF may induce toxicity at higher

concentrations, underscoring the need to optimize its dose, while IKVAV, REDV, and GFOGER demonstrated favorable biocompatibility. These peptides showed a dose- and time-dependent viability profile for endothelial cells to allow tuning the interface of the biomaterial. GFOGER was found to promote cell proliferation more efficiently than IKVAV and REDV. The inhibitory effect on cell metabolic activity arising from the microenvironment was mitigated in the presence of IKVAV and REDV, suggesting a protective or stabilizing role of the peptide motifs. Collectively, these findings offer a comprehensive investigation of common peptide motifs for selecting and tuning these cues to engineer biointerfaces in next-generation biomaterial designs such as stents, vascular grafts, patches, or dressings.

Keywords: peptide, surface modification, functional biomaterials, interface, electrospinning, tissue engineering

1. INTRODUCTION

Biomaterials are used to augment or replace any tissue, organ, and biological function in the body. They have existed since the earliest periods of human history [1]. Interaction between the material and host tissue plays a central role, indeed the interface governs the cell fate and the overall performance of biomaterials in the body. Over time, the bioinert first -generation biomaterials were converted to bioactive and bioresorbable materials, where they can react and form stable bonds with tissue for a specific response. Then an era began in which materials were engineered to promote and enhance specific cellular activity at the molecular level for regeneration [2–4]. During this evolution of biomaterials, interest in surface properties of materials was increased. To achieve the aims of tissue engineering, scaffolds are integrated with living cells or biomolecules from cellular components, resulting in interactions between cells and materials that create an enhanced site-specific functional interfacial surface [2,3]. Extracellular matrix (ECM) is the key component of all tissues and organs, which provides a 3D network for physical support and creates a special niche for cellular activities, therefore mimicking the structure and function of ECM may facilitate tissue regeneration. Electrospinning is a prominent technique to fabricate scaffolds due to its capability to mimic native ECM fibrils and interconnected porous structures, as well as its ease of use and a large range of

suitable polymer sources. These fibrous networks and interconnected pores ensure a large surface area that are influential for cell migration and proliferation [5–7]. However, providing a natural-like environment and mechanical support to cells are not sufficient since the native ECM also regulates cell adhesion, proliferation, differentiation, tissue regeneration and remodeling with biochemical and biophysical cues that create a special surroundings. Uncovering cell–ECM interactions enables control over these processes and facilitates the translation of these biochemical and biophysical cues into biomaterial design through engineering strategies. In this regard, the material surface serves as the primary platform for mimicking and initiating desired cellular behaviors, as these interactions are initiated at the material interface first [8–10]. Polymeric biomaterials are one of the major classes in tissue engineering. Even though natural polymeric materials have high biocompatibility and biological cues for cell interaction, their low mechanical characteristics and short half-life highlight the synthetic materials. Synthetic polymeric materials offer tunable and excellent mechanical integrity, however do not possess substrates to trigger cell activities. Hence, conjugation of functional groups or biomolecules such as ECM proteins, peptides, growth factors are of interest for improving biomaterials in terms of enhanced biocompatibility and mimicking cellular activities [11,12]. This study aimed to synergize the mechanical features and ECM mimicking architecture of electrospun scaffolds with biofunctional surface engineering through peptide conjugation. Although numerous studies have investigated individual bioactive peptides, comparative evaluation of distinct biofunctional peptide motifs for vascular niche conjugation on a common electrospun scaffold platform remains limited, particularly for cardiovascular applications. Therefore, this work established a small but functionally diverse peptide library to systematically investigate how peptide mediated interfaces influence endothelial-related early cellular responses, peptide biocompatibility, and scaffold associated biological interactions. Electrospun scaffolds composed of PLGA were manufactured since PLGA offers excellent biocompatibility, mechanical integrity, and biodegradability, and it is already approved for human use by regulatory bodies [13]. Furthermore, PLGA possesses terminal carboxyl groups that allow facile surface modification of peptides through either physical adsorption or chemical conjugation. We synthesized five peptide motifs inspired by the literature: 1) laminin-derived IKVAV, 2)

fibronectin-derived REDV, 3) collagen-mimicking GFOGER, 4) bivalirudin-derived (D-Phe)PRP, and 5) laminin-1-derived KAFDITYVRLKF, which might be promising biomolecules for in-use cardiovascular applications. The first peptide motif, IKVAV, has been investigated for its ability to enhance proliferation and attachment of endothelial cells in addition to angiogenesis [14–18], but its use specifically in vascular grafts is limited. The second peptide motif, REDV, has been widely studied due to its endothelial cell–selective adhesion properties, fibrin clot reduction, and its potential to enhance endothelialization while minimizing smooth muscle cell and platelet attachment on surfaces [19–22]. The third peptide, CGFOGER, present in collagen type I, II, IV, VII, and XI, has attracted significant attention as a key cell-adhesive sequence [23–25]. It displays a high-affinity binding site in collagens I and IV for α2β1 integrin which plays a key role in angiogenesis [26,27] as well as platelet activation. This motif was also found to be effective in reducing vascular calcification and osteogenic switching in vascular smooth muscle cells [28]. The fourth peptide, (D-Phe)PRP, is a domain of bivalirudin, which is a direct thrombin inhibitor, and this domain binds to the thrombin active site [29]. Studies confirm that incorporating the highly effective anticoagulant bivalirudin, or its thrombin-binding peptide motif ((D-Phe)PRP), onto vascular graft surfaces significantly improves hemocompatibility and patency by inhibiting platelet and fibrin adhesion/activation [30,31]. The laminin γ1 chain-derived peptide motif, C16 (KAFDITYVRLKF), is a potent proangiogenic agent that promotes endothelial cell adhesion and capillary-like tube formation. Recent studies demonstrate that its co-delivery with anti-inflammatory peptides via a scaffold synergistically enhances angiogenesis, muscle regeneration, and perfusion recovery while mitigating detrimental inflammation in models of peripheral artery disease [32–37]. The peptide library in this study was established to comparatively investigate motifs with potential relevance for vascular niche engineering. In detail, IKVAV and REDV motifs were selected due to their reported roles in endothelial cell attachment and endothelialization-related responses. Among the adhesion-related motifs, the GFOGER motif was intentionally included because it targets distinct integrin-mediated interactions. The (D-Phe)PRP motif was included due to its thrombin-binding and antithrombotic functionality, whereas the KAFDITYVRLKF motif was selected based on its proangiogenic property. Herein, we synthesized these five distinct peptides modified at

N-terminus with a cysteine residue and systematically conjugated this small library of peptide motifs onto maleimido-functionalized electrospun PLGA scaffolds. Among various surface modification strategies, [38] thiol–maleimide chemistry provides high selectivity and reactivity which enables homogeneous and oriented peptide conjugation while minimizing undesirable alterations in material properties. Such Michael-type addition reactions are rapid and efficient at low reagent concentrations making them suitable for controlled biointerface functionalization of electrospun scaffolds [39,40]. The resulting functionalized electrospun scaffolds were characterized for conjugation efficiency, surface properties, and cellular responses and were intended to serve as a complementary layer or a bulk-modified biomaterial providing the initial platform for cell-material interactions. Hence, the cytotoxicity of peptide motifs and the biocompatibility of peptide-functionalized scaffold were comprehensively investigated in both fibroblast and endothelial cells *in vitro*, providing critical insight into the interface engineering of next-generation biomaterials such as cardiovascular patches, stents, vascular grafts or dressings. The proposed strategy enables controlled and comparative investigation of peptide-mediated cellular responses while highlighting the importance of peptide dose optimization and tunable biointerface functionalization for the rational design and future translation of cardiovascular biomaterials.

2. MATERIALS AND METHODS

2.1. Materials

The solvents for peptide synthesis were used without additional purification. Fmoc-amino acids, Oxyma Pure, N,N-diisopropylethylamine (DIEA) and 1,1,1,3,3,3-Hexafluoro-2-propanol (HFIP) were purchased from Fluorochem (Hadfield, United Kingdom). Rink amide AM resin (100–200 mesh, 0.7 mmol/g) was received from Novabiochem (Läufelfingen, Switzerland). Diisopropylcarbodiimide (DIC) and 1-(3-Dimethylaminopropyl)-3-ethylcarbodiimide (EDC) were purchased from ABCR GmbH (Karlsruhe, Germany). N-Hydroxysuccinimide (NHS) was received from Tokyo Chemical Industry Europe N.V. (Zwijndrecht, Belgium). Dimethyl sulfoxide (DMSO) was acquired from PanReac AppliChem ITW Reagents (Darmstadt, Germany). Fmoc-l-trans-Hyp(tBu)-OH was supplied from Iris Biotech GmbH (Marktredwitz, Germany). Dimethylformamide

(DMF), Piperidine,Thioanisol, Trifluoroacetic acid (TFA), 3,6-dioxa-1,8-octanedithiol(DODT), 1-(2-aminoethyl)maleimide hydrochloride, carboxyl terminated PLGA (L:G 50:50, Mw:66kDa, PURASORB®), tris(2-carboxyethyl)phosphine (TCEP), 2-Morpholinoethanesulfonic acid monohydrate (MES), phosphate buffered saline (PBS; pH:7.4), acetonitrile(≥99.9%, gradient grade), Dulbecco's Modified Eagle Medium high glucose (DMEM), Trypsin-EDTA, 3-(4,5-dimethylthiazol-2-yl)-2,5-diphenyltetrazolium bromide powder (MTT) were provided from Sigma-Merck (Darmstadt, Germany). Diethyl ether was provided from Honeywell- Riedel-de Haën (Seelze, Germany). Fetal bovine serum (FBS) was supplied from ATCC (Manassas, Virginia, USA). Penicillin-streptomycin (Gibco; 10,000 U/mL), Live/Dead staining kit (Invitrogen), 4′,6-diamidino-2-phenylindole (Invitrogen; DAPI), and Alexa Fluor 488 phalloidin (Invitrogen) were purchased from Thermo Fisher Scientific (Waltham, MA, USA). Normal human dermal fibroblasts (nHDFs) were provided by PromoCell (Heidelberg, Germany) and human umbilical vein endothelial cells (HUVECs) by Innoprot (Derio, Bizkaia, Spain). nHDFs were cultured at 37°C with 5% CO_2 in a 25 cm^2 culture flask with DMEM containing 1% (v/v) penicillin–streptomycin and 10% (v/v) FBS. HUVECs were cultured in endothelial cell medium provided by Innoprot composed of basal medium, 1% (v/v) penicillin–streptomycin, 10% (v/v) FBS and 1% endothelial cell growth supplement.

2.2. Peptide synthesis and purification

The chemical structures of each peptide are given in the supplementary information (SI) as Fig. SI1. The peptides were synthesized on CEM Liberty Blue synthesizer (Matthews, NC, U.S.A.) using F-moc Solid Phase Peptide Synthesis on Rink amide AM resin (0.7 eq/g) loading) at 0.1 mmol scale. The amino acid concentration was 0.2 M in DMF. The coupling was carried out in the presence of 1 M Oxyma and 0.5 M DIC in DMF. All the amino acids were coupled at 75°C using 170 W for 15 s and then at 90°C using 40 W for 110 s. Deprotection was performed at 75°C using 155 W for 15 s and then at 90°C using 50 W for 50 s. 20% Piperidine in DMF was used as a deprotecting agent. The cleavage was then performed using 4 mL of cleavage cocktail for each peptide (TFA/Thioanisol/DODT; 90:7:3) for 3 h at room temperature. After the cleavage, the peptides were precipitated from ice-cold diethyl ether and recovered by centrifugation at 4°C. Three diethyl ether washes/centrifugation cycles were carried out to efficiently

remove the scavengers, and the peptides were dried under N_2 gas. Peptides were purified using an ADAMAS C-18 column from Sepachrom (10 µm, 250 × 21.2 mm) by reverse phase-high performance liquid chromatography (RP-HPLC) using a gradient elution of 5% to 70% solvent B (solvent A: water/trifluoroacetic acid 100:0.1; solvent B: acetonitrile/trifluoroacetic acid 100:0.1) over 40 min at a flow rate of 10 mL/min. The purified peptides were freeze-dried and stored at 0°C. Afterwards, they were analysed using analytical HPLC (5% B for 3 min; 5% to 70% B over 20 min), and Mass spectra were acquired on a Fisons MD800 spectrometer and electrospray ion trap on a Finnigan LCQ advantage thermo-spectrometer [41]. Each peptide sequences CIKVAV-NH_2, CREDV-NH_2, CGFOGER-NH_2, C(D-Phe)PRP-NH_2, CKAFDITYVRLKF-NH_2- abbreviated throughout the rest of work as P1, P2, P3, P4 and P5 respectively.

2.3. Electrospun scaffold fabrication and characterization

PLGA (50:50, Mw:66kDa, PURASORB®) polymer solution was prepared in HFIP at 25% w/v concentration and dissolved by stirring overnight in a tightly sealed glass vial. Electrospinning was performed using a NANON 01A vertical electrospinning device (MECC Co. Instruments Ltd., Fukuoka, Japan) on a flat aluminum collector with a 0.1 mL/h flow rate and 15 kV voltage for 2 h. A 22G blunt-type needle was used, and the collector-needle distance was kept at 15 cm. Scaffolds were left dry under the hood overnight to evaporate residual HFIP. Electrospun scaffold thickness was measured by a caliper. Hereafter, electrospun PLGA scaffolds without peptide incorporation were abbreviated as “plain scaffolds.”

2.3.1. Morphological and mechanical characterizations of plain scaffolds

Morphology and homogeneity of the plain scaffold were evaluated and confirmed with scanning electron microscopy (SEM, Mira3 XMU, Tescan, Brno – Kohoutovice, Czech Republic). Scaffolds were sputtered with gold before, and images were taken under 20kV at several magnifications. The fiber diameter distribution of all scaffolds was quantitatively analysed on at least 100 fibers using ImageJ software [42].

Mechanical features of plain scaffolds were further characterized. First, plain scaffolds were cut into dog-bone shapes with a calibrated cutter according to ASTM D-882 standard. Then, load and travel values of scaffolds were measured with a uniaxial tensile

machine (Mark-10 Tensile Testers, Copiague, NY, USA) in triplicate at 20.1 mm/min upward speed. Stress and strain values were calculated according to Eq. 1 and Eq. 2. below.

$$\sigma = \frac{F}{A} \quad \text{Eq. 1}$$

$$\varepsilon = \frac{\Delta L}{L0} \quad \text{Eq. 2}$$

where

σ is stress (MPa), F is the applied force (N), A is cross sectional area (mm^2), ε is strain (mm/mm), ΔL is displacement (mm), L_0 is the initial sample length (mm).

2.4. Peptide conjugation on plain scaffolds

Initially, the surfaces of the plain scaffolds were functionalized with 1-(2-aminoethyl) maleimide hydrochloride as a linker to enable the crosslinking of cysteine-containing peptides onto the scaffolds via a maleimide–thiol reaction (Fig. 1) [40,43]. Plain scaffolds were cut into a circular shape with a diameter of 15 mm and weighed. Scaffolds were incubated with 2mM EDC and 5 mM NHS (solutions prepared in MES buffer (0.1 M, pH 5-6) for 2 h at room temperature. Subsequently, activated surfaces of plain scaffolds were treated with maleimide linker (10 equivalents relative to the scaffolds' weights) in MES buffer (0.1 M, pH 5-6), and 5µl DIEA was added. –COOH-activated surfaces of fiber scaffolds were exposed to the linker overnight (16-18h) at room temperature. After that, each sample was transferred gently and washed with MQ water 2-3 times to remove residuals. Peptide solutions (3 equivalents relative to the PLGA equivalents) were prepared in PBS (1x; pH 7.4), including TCEP (2 equivalents of peptide) as a reducing agent to prevent disulfide bond formation and were stirred for 30 min. Then, peptide conjugation onto the scaffolds was accomplished by reacting with the maleimide-functionalized surfaces with thiol-containing peptides for 4 h at room temperature. After conjugation was completed, fiber scaffolds were removed from peptide solutions and washed with PBS twice. Peptide solutions obtained initially and following the conjugation process were collected and preserved for subsequent indirect quantification of peptide

conjugation. Corresponding peptides conjugated onto the plain scaffolds will hereafter be referred to as P1-scaffold, P2-scaffold, P3-scaffold, P4-scaffold, and P5-scaffold.

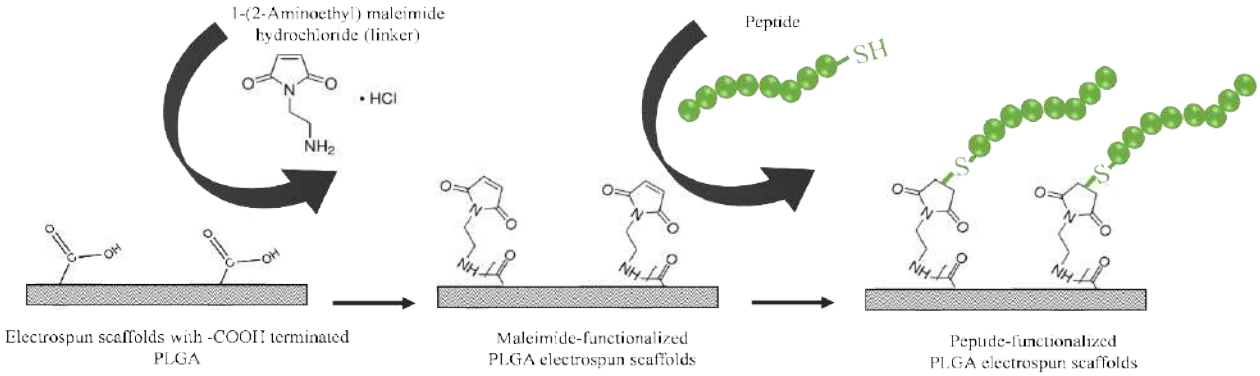

Fig. 1: Schematic representation of peptide conjugation on plain scaffold.

2.5. Physicochemical characterizations after peptide conjugation

2.5.1. Morphological evaluations of peptide-conjugated scaffolds

Morphology and homogeneity of P1-scaffold, P2-scaffold, P3-scaffold, P4-scaffold, and P5-scaffold were evaluated and confirmed with scanning electron microscopy (SEM, Mira3 XMU, Tescan, Brno – Kohoutovice, Czech Republic). Scaffolds were sputtered with gold before, and images were taken under 20kV at several magnifications. The fiber diameter distribution of all scaffolds was quantitatively analyzed using ImageJ software [42] before and after peptide conjugation.

2.5.2. Quantification of peptide conjugation onto plain scaffolds

Gradient HPLC (1260 Infinity, Agilent Technologies, Santa Clara, USA) was employed to analyse peptide conjugation. The analyses were conducted with a C18 reversed-phase column (150 × 4.6 mm, 5 µm). The mobile phase was acetonitrile and MQ water containing 0.1% TFA. The gradient program started with 5% acetonitrile, followed by a linear increase to 70% at 20 min, a linear increase to 90% at 25 min, and completed with a drop to 5% at 30 min. The flow rate was 0.8 mL/min, the column temperature was maintained at 25 °C, and detection was performed at 220 nm [41]. Calibration curves for each peptide were constructed based on the area under the curve (AUC) from chromatograms, using concentrations between 25 and 500 µg/mL in PBS (1X, pH 7.4)

under the aforementioned HPLC parameters. Peptide solutions (see *Section 2.4*) were analyzed, and the peptide amount conjugated to the scaffold, together with the conjugation efficiency, was calculated by following Eq. 3, Eq. 4 and, Eq. 5.

$$\text{Conjugated peptide amount (μg)} = (C_I - C_F) \times V \quad \text{Eq. 3}$$

where C_i and C_F represent the initial and final peptide concentrations, respectively, and V is the solution volume.

$$\text{Conjugation efficiency (\%)} = \frac{Conjugated\ peptide\ (nmol)}{plain\ scaffolds\ (nmol)} \times 100 \quad \text{Eq. 4}$$

where:

$$\text{Plain scaffolds (nmol)} = \frac{average\ weight\ of\ PLGA\ fiber\ scaffolds(g)}{PLGA\ molecular\ weight\ (gmol{-}1)} \times 10^9 \quad \text{Eq. 5}$$

2.5.3. Relative water absorption and surface wettability of peptide-conjugated scaffolds

Based on the results presented in Sections 3.4 and 3.6, only P1-scaffold, P2-scaffold, and P3-scaffold were included in the relative water absorption and surface wettability analyses, while P4- and P5-functionalized scaffolds were excluded due to the relatively low conjugation efficiency of P4 and the cytotoxic effects observed for P5. Circular specimens of P1-scaffold, P2-scaffold, and P3-scaffold (Ø: 15 mm) were stored in a desiccator for at least 72 h to remove residual moisture before being used in experiments. To perform relative water absorption, the scaffolds were weighed (W_0) and subsequently immersed in MQ water for 24 h at room temperature. After gently removing superficial water from the scaffold surfaces, they were weighed again (W_1), and the relative water absorption was calculated by the following Eq. 6.

$$\text{Relative water absorption (\%)} = \frac{W_1 - W_0}{W_0} \times 100 \quad \text{Eq. 6}$$

Statistical analyses were performed using GraphPad Prism v8.4.2, applying ordinary one-way ANOVA followed by Dunnett's multiple comparisons test. Surface wettability of fiber scaffolds before and after peptide conjugation was evaluated by contact angle measurements. 5 μL of MQ water was dropped onto each scaffold surface. The experiment was performed in triplicate, and water droplets were placed at three different locations on each scaffold. Surface contact angles were measured using ImageJ software

with low-bond axisymmetric drop shape analysis. Statistical analyses were carried out using GraphPad Prism v8.4.2, applying ordinary one-way ANOVA followed by Dunnett's multiple comparisons test.

2.6. *In Vitro* evaluations on normal human dermal fibroblasts (nHDFs)

2.6.1. Cytotoxicity of peptides

Cytotoxicity tests for P1, P2, P3, and P5 were performed on nHDFs. nHDFs were seeded in standard 96-well plates at a density of 1×10^4 cells per well in complete culture medium (DMEM supplemented with 10% FBS and 1% penicillin–streptomycin). The cells were then incubated overnight to allow for proper adherence. Each peptide solution was prepared under sterile conditions and diluted to various concentrations (8–400 μM) in complete cell culture medium. Before treatment, nHDFs were washed twice with PBS to remove dead cells. The cells were then exposed to diluted peptide solutions for 24 h. Following incubation, cell viability was assessed using the MTT assay.

2.6.2. Cell viability assay (Live/Dead staining) and Immunofluorescence staining (DAPI and Phalloidin) of peptide-conjugated scaffolds on nHDFs

To investigate the interaction between fibroblast cells and peptide-conjugated fiber scaffolds, cell viability and morphology were evaluated on selected peptide-conjugated scaffold surfaces using Live/Dead staining and DAPI/Phalloidin staining, respectively. P1-scaffold, P2-scaffold, and P3-scaffold underwent surface UV sanitization for 1 h. These scaffolds were placed in sterile cell crowns to hinder floating during incubation. $5x10^3$ nHDFs were seeded per scaffold and were incubated for 3 days. After incubation, Live/Dead and DAPI/Phalloidin staining were performed according to the manufacturer's protocol [44–46].

2.7. *In Vitro* evaluations on human umbilical vein endothelial cells (HUVECs)

2.7.1. Cytotoxicity and cell proliferation assessment of peptides

To investigate the dose-dependent effects of P1, P2, and P3 on immortalized HUVECs' viability and proliferation, cells were seeded at a density of 3,000 cells/well in standard 96-well plates and incubated for 3 days to allow cell attachment and proliferation. P1, P2,

and P3 peptides were diluted in endothelial cell culture medium at different concentrations (8–400 μM; 10 -200 μg/mL) and filter-sterilized prior to use. HUVECs were treated with the peptide-containing media for 24 h and 72 h. Following treatment, peptide solutions were aspirated at 24 h and 72 h, and cells were washed twice with PBS to remove residual peptides. Subsequently, cells were subjected to the MTT assay to assess viability. Cells treated with fresh medium without peptides were used as the control group. Statistical analyses were performed using GraphPad Prism v8.4.2, applying ordinary one-way ANOVA followed by Sidak's multiple comparisons test.

2.7.2. Cytotoxicity and cell proliferation assessment of peptide-conjugated scaffolds

To assess the potential release of cytotoxic and inhibitory substrates from peptide-conjugated scaffolds, cytotoxicity and proliferation profile of P1-scaffold, P2-scaffold, and plain scaffolds were evaluated by employing extraction method on HUVECs. Cells were seeded at a density of 3.000 cells/ well in 96-well plates and incubated for 3 days prior to treatment. Peptide-conjugated scaffolds (P1-scaffold and P2-scaffold) and plain scaffolds were sterilized by UV irradiation on each side (total exposure time of 70 min), followed by washing with 70% ethanol and with PBS twice each. The scaffolds were then immersed in endothelial cell culture medium at a concentration of 5 mg/mL (fiber mass to medium volume) and incubated for 3 days at 37 °C to obtain scaffold extracts. Culture medium incubated under identical conditions without scaffolds was used to have control extracts. After incubation, cells were washed twice with PBS and subsequently treated with the filter-sterilized scaffold extracts or control medium. Cell viability was assessed after 24 h and 72 h using the MTT assay. Statistical analyses were performed using GraphPad Prism v8.4.2, applying ordinary one-way ANOVA followed by Sidak's multiple comparisons test.

3. RESULTS

3.1. Peptide synthesis and purification

The purity of the synthesized peptides was analyzed using HPLC (see Fig. SI2), and their molecular weights were confirmed with mass spectroscopy (see Fig. SI3). The purity (%), experimental molecular weight (MW exp), calculated theoretical molecular weight (MW cld), and recovered final mass of each peptide sequence are summarized in Table 1 below. HPLC results revealed that peptides were synthesized with high purity. MW exp results of

each peptide obtained from mass spectroscopy matched the calculated theoretical values. Specifically, the mass spectrometric data may seem to indicate a pronounced discrepancy between the MW cld and MW exp of P5; however, this apparent offset reflects detection of the peptide in a multiply charged state and is consistent with the doubly charged ion $[M+2H]^{2+}$ of the target peptide.

Table 1: Peptide purity and quantity.

Name	Peptide Sequence	Role	MW exp ($gmol^{-1}$)	MW cld ($gmol^{-1}$)	Purity (%)	Mass (mg)
P1	CIKVAV-NH_2	Promoting endothelial cell proliferation, attachment and angiogenesis	631.79	630.39	94%	41.2
P2	CREDV-NH_2	Promoting endothelial cell adhesion	620.06	619.27	100%	58.8
P3	CGFOGER-NH_2	Promoting cell adhesion	780.96	779.34	99%	69.8
P4	C(D-Phe)PRP-NH_2	Trombin binding site (Anticoagulation)	619.39	617.31	99%	77.5
P5	CKAFDITYVRLKF-NH_2	Pro-angiogenesis	803.05	1601.88	95.3%	27.5

3.2. Morphological and mechanical characterizations of plain scaffolds

Fiber morphology was evaluated by SEM, and a uniaxial tensile test was performed to demonstrate the mechanical characteristics of plain scaffolds. Representative SEM image in Fig. 2 confirmed that randomly oriented, straight, and continuous plain fibers were produced without bead formation. The fiber diameter distribution was revealed as 2.9 ± 0.2μm for plain scaffolds. The thickness of scaffolds was measured as 107.2 ± 18.2

μm (n=10). Ultimate tensile stress (UTS), Young's modulus, yield strength, yield strain, breaking point, and elongation at break were determined and listed in Table 2.

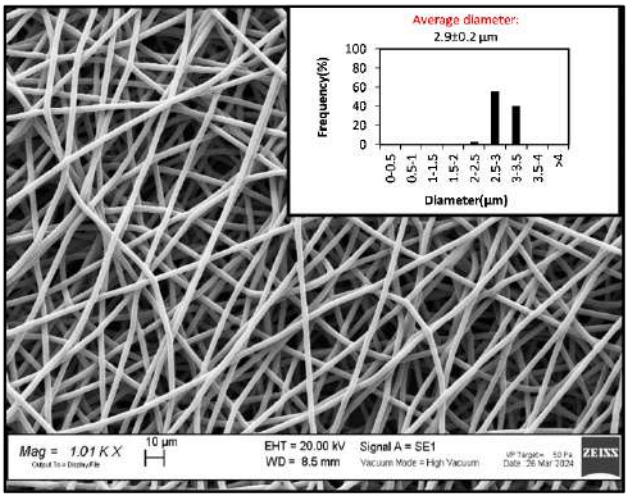

Fig. 2: SEM image of a plain scaffold.

Table 2: Mechanical characterization of plain scaffold (average ± standard deviation).

UTS (MPa)	Young modulus (MPa)	Yield strength (MPa)	Yield strain (%)	Breaking point (MPa)	Elongation at break (%)
2.9 ± 0.1	54.2 ±14.6	1.8 ± 0.2	3.1 ± 0.3	2.6 ± 0.1	442.7 ± 48.7

These results indicate that the scaffolds possess flexibility as well as stiffness, comparable with the mechanical response from electrospun PLGA matrices. Literature studies revealed a variety of Young's modulus and UTS results for electrospun PLGA membranes, ranging between 36-85 MPa and 3.2-5.4 MPa, respectively, due to various solvent/polymer systems, ratio of lactic acid to glycolic acid, molecular weight, and electrospinning parameters [47–51]. The plain scaffold exhibited UTS as 2.9 ± 0.1 MPa and Young's modulus 54.2 ± 14.6 MPa and may indicate a moderate stiffness and mechanical strength, which are desirable to ensure handling stability during implantation of biomaterials and to provide a mechanically robust platform for subsequent peptide functionalization. As shown in Fig. 3, the yield point was followed by a strain hardening region where the scaffold became mechanically stronger upon deformation. This suggests that the electrospun PLGA network is capable of redistributing the stress and

progressive fiber alignment under tensile loading. High ductility of the scaffolds with 442.7 ± 48.7% elongation at break is particularly advantageous, as it allows structural adaptability without premature failure. Such behaviors support the suitability of the scaffold as a mechanically resilient platform and prevent the catastrophic failure of biomaterials. These findings collectively demonstrate that electrospun plain scaffold can provide sufficient mechanical integrity, even without reinforcement, and is beneficial where materials are subjected to continuous deformation and mechanical loading, as well as exhibit tissue remodeling processes without structural failure.

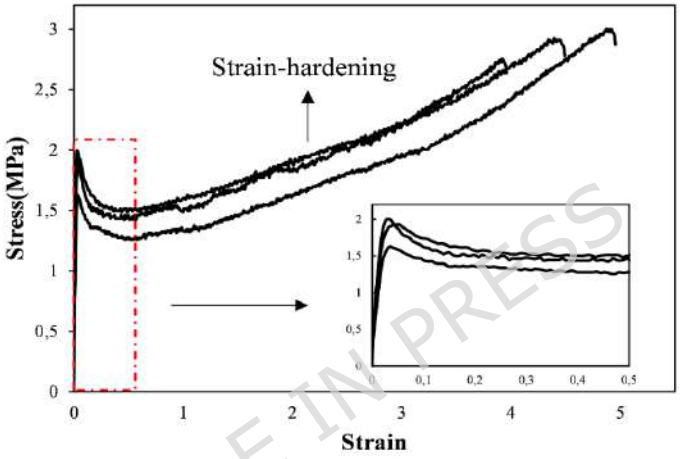

Fig. 3: Representative stress-strain curve of plain scaffolds.

3.3. Morphological evaluations of peptide-conjugated scaffolds

The morphology of peptide-conjugated scaffolds was evaluated, and their SEM images in Fig. 4 (A-E) showed that peptide conjugation on the scaffold surface did not cause any change, and all peptide-conjugated scaffolds have similar morphology to plain scaffolds (Fig. 2), except for the presence of whitish salt crystals on peptide-conjugated scaffolds resulting from the washing procedure with PBS after crosslinking. Moreover, average fiber diameters of P1-scaffold, P2-scaffold, P3-scaffold, P4-scaffold, P5-scaffold were measured as 2.6 ± 0.1μm, 2.2 ± 0.2μm, 2.8 ± 0.02 μm, 2.7 ± 0.02 μm and 2.0 ± 0.023 μm, respectively.

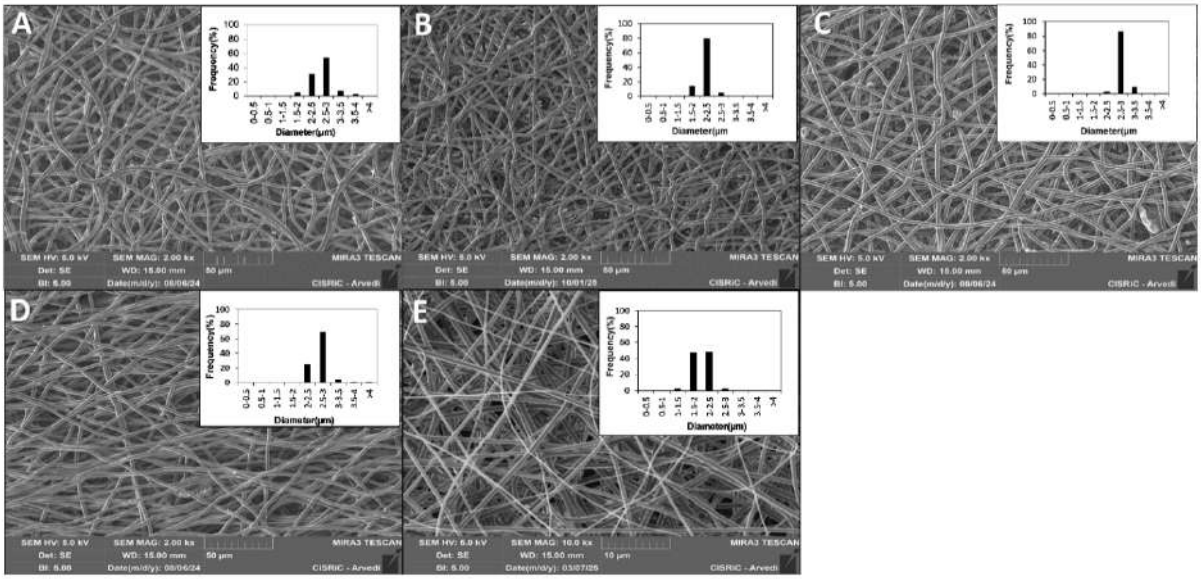

Fig. 4: SEM images and fiber diameter distribution of (A) P1-scaffold, (B) P2-scaffold, (C) P3-scaffold, (D) P4-scaffold, (E) P5-scaffold.

3.4. Quantification of peptide conjugation onto plain scaffolds

Peptide conjugation onto the plain scaffolds was quantified by HPLC measurements. Conjugation efficiency was calculated as the ratio of the conjugated peptide amount (nmol) to the plain scaffolds (nmol), expressed as a percentage. The results are summarized in Table 3.

Table 3: Conjugated peptide amount on scaffold surfaces.

Name	Peptide conjugation (nmol)	Peptide conjugation (μg/mg fibers)	Conjugation efficiency (%)
P1-scaffold	18.9 ± 0.30	6.6 ± 1.1	36.8 ± 6.4
P2-scaffold	15.7 ± 0.58	4.7 ± 1.6	26.8 ± 9.3
P3-scaffold	28.5±1.68	4.6±1.8	21.1± 8.3
P4-scaffold	22.3±6.9	1.8±0.5	10.4 ± 3.1
P5-scaffold	12.9 ± 0.66	9.1 ± 2.7	24.9 ± 11.1

Among the tested peptides, P1-scaffold exhibited the highest conjugation efficiency (36.8 ± 6.4%), while P4-scaffold showed the lowest efficiency (10.4 ± 3.1%). We attribute these differences to cysteine accessibility, steric constraints, and peptide physiochemistry (net charge/hydrophobicity), which govern thiol–maleimide interaction at the plain scaffolds' interface. Specifically, low conjugation efficiency exhibited with P4 may arise from the contiguous of the cysteine-phenylalanine motif, which might suppress the Thiol-Michael addition due to the steric shielding effect. The rigid aromatic ring of phenylalanine adjacent to the cysteine residue may act as a physical barrier and may restrict the spatial accessibility. In addition, possible π-thiol interactions may reduce the conformational flexibility, thereby reducing the reactive accessibility of the cysteine thiol group during conjugation [52]. Further studies will focus on peptide solubility and conformational behavior during surface conjugation. In this study, the surface modification achieved with P4 was considered insufficient to provide a meaningful scaffold-based biological evaluation for reliable comparison with the other peptide functionalized scaffolds. Therefore, P4 was excluded from further experiments and was not subjected to subsequent *in vitro* evaluations, including cytotoxicity and cell proliferation studies.

3.5. Relative water absorption and surface wettability of peptide-conjugated scaffolds

P1-scaffold, P2-scaffold, and P3-scaffold were evaluated for relative water absorption and wettability characteristics. Water absorption capacity of plain scaffold, P1-scaffold, P2-scaffold, and P3-scaffold, relative to their starting dry weight, was calculated and shown in Fig. 5 as 220.8 ± 21.8%, 210.0 ± 14.3%, 145.9 ± 36.2%, 139.3 ± 58.7%, respectively. A slight descending trend was observed in proportion with peptide conjugation efficiency on scaffolds. Following peptide conjugation, partial consumption of terminal hydroxyl and carboxyl groups and the introduction of hydrophobic moieties may reduce the number of available hydrogen-bonding sites and cause a decrease in water absorption. Despite a modest decrease in water absorption, the results did not indicate a significant alteration in the water absorption capacity of scaffolds. This indicates that the surface modification induced minor changes in interfacial hydrophilicity without changing the bulk features of electrospun scaffolds. Furthermore, the surface wettability of all scaffolds was examined and presented in Fig. 5. The contact angle for the plain scaffold was 121.3 ± 3.8°, similar

to values reported in literature [50,53]. P1-scaffold, P2-scaffold, and P3-scaffold were measured as 120.5 ± 6.5°, 104.17 ± 3.9°, 118.5 ± 1.2°, respectively.

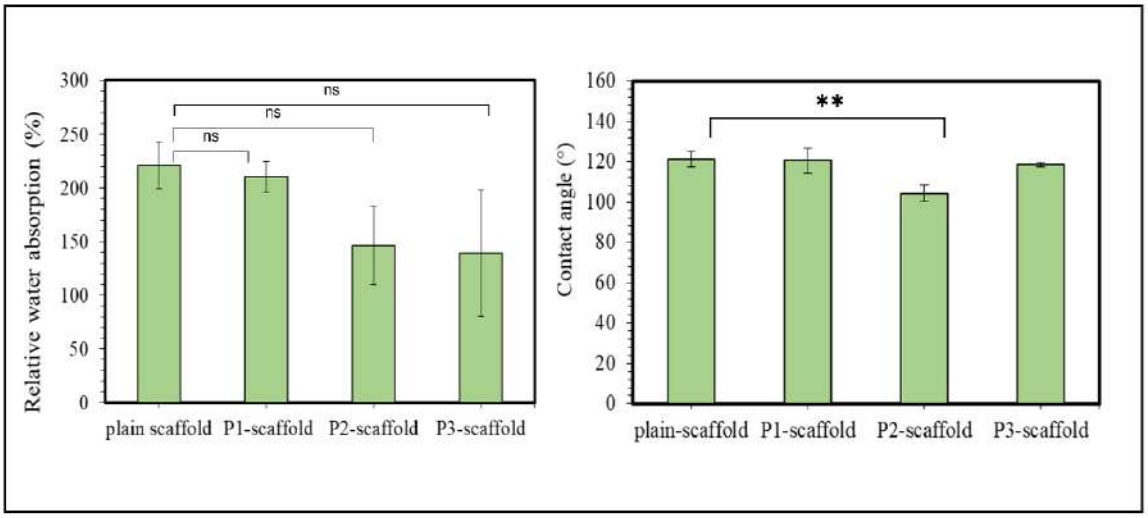

Fig. 5: Relative water absorption capacity and surface wettability of peptide-conjugated scaffolds. Statistical significance was defined as follows: ns, not significant ($p \geq 0.05$); *$p < 0.05$, significant; **$p < 0.01$, very significant; ***$p < 0.001$, extremely significant; and ****$p < 0.0001$, extremely significant.

The hydrophilicity of the peptide sequences was estimated using the GRAVY (Grand Average of Hydropathy) index based on the Kyte–Doolittle scale and calculated by the following Eq. 7 below. GRAVY index of P1, P2, and P3 was calculated as 2.21, -0.96, and -0.6, respectively. According to the GRAVY index, the hydrophilicity of the peptides followed the order P2 > P3 > P1, where higher GRAVY values correspond to increasing hydrophobicity. Consistent with this, modification of the P2 peptide improved significantly scaffold surface wettability.

$$\text{GRAVY index} = \frac{sum\ of\ Kyte{-}Doolittle\ value\ of\ residues}{number\ of\ residues\ in\ the\ peptide} \quad \text{Eq. 7}$$

3.6. Cytotoxicity of peptides on nHDFs

Cytotoxic effect of peptide solutions (P1, P2, P3, and P5) was investigated on nHDFs for 24 h. The P4 (C(D-Phe)PRP-NH_2) experimental group was not performed due to its low conjugation efficiency on the plain scaffold surface, as shown in Table 3. Results showed that in Fig. 6, the P1, P2, and P3 groups did not exhibit toxic effects on fibroblasts and confirmed their biocompatibility. Cell viability of P1 and P2 groups remained between 80%

and 100% up to the highest concentration, with a slight decrease in P2 below the threshold (80%) at the concentration of 32μM. With P3, cell viability reached over 100% at even low concentrations and maintained the viability above the threshold at high concentrations. Interestingly, P3 not only maintained cell viability but also triggered fibroblast proliferation compared to P1 and P2. However, Garcia et al. demonstrated that a triple-helical peptide containing a P3 motif (GGYGGGP(GPP)5GFOGER(GPP)5GPC) functionalized hydrogels enhanced vascularization and bone regeneration more effectively than RGD-based hydrogels, even in the absence of VEGF, and that the level of vascularization was independent of VEGF dose [27]. These findings indicate that the P3 motif can promote angiogenesis, even in the absence of VEGF, highlighting its potential as a pro-angiogenic cue for vascular graft applications. The P1 and P2 motifs enhance endothelial cell adhesion and growth rather than fibroblast proliferation, as reported in previous studies [14,19,22]. In contrast, cell viability dropped below 80% already at 16 μM with P5, then remained at ~80% and further decreased to ~50-60% at 159–396 μM. Our results revealed a dose-dependent cytotoxicity on fibroblasts with the P5 motif. Similarly, it was shown that P5 has the strongest and dose-dependent inhibitory effect for endothelial cells in comparison with other laminin-1 derived motifs, in the presence of laminin-1 *in vitro* [54]. Although the exact mechanism underlying the inhibitory effect of the P5 peptide was not investigated in the present study, bioactive peptides may induce cytotoxicity through membrane disruption, pore formation, necrosis, apoptosis-related membrane interactions, or intracellular mitochondrial targeting pathways [55,56]. Therefore, saturation of integrin with excessive peptide may have disrupted normal integrin-mediated cellular interactions and signaling balance, while the presence of positively charged and hydrophobic residues within the P5 motif may also have damaged the cell membrane. In addition, uptake of elevated peptide concentrations may have induced cellular stress and altered the local chemical microenvironment such as osmotic imbalance and pH changes, collectively contributing to reduced cellular metabolic activity and viability.

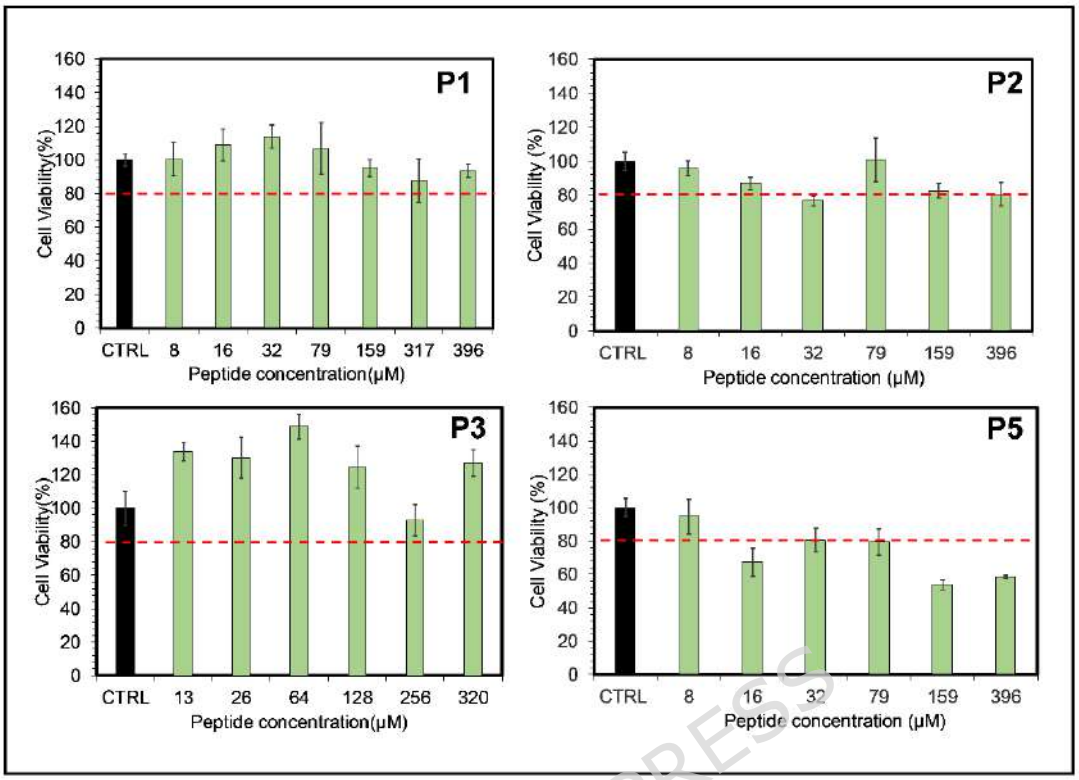

Fig. 6: Cell viability of peptide (P1, P2, P3, P5) solutions at various concentrations.

3.7. Cell viability assay and (Live/Dead staining) Immunofluorescence staining (DAPI and Phalloidin) of peptide-conjugated scaffolds on nHDFs

Cell viability and morphology were assessed on peptide-conjugated fiber scaffolds (P1-scaffold, P2-scaffold, and P3-scaffold) with Live/Dead and Immunofluorescence staining. As reported in the results section 3.4 and 3.5, the outcomes of the low conjugation efficiency of P4 and reduced cell viability caused by P5 indicated that only peptides P1, P2, and P3 were the most suitable for further investigation. Accordingly, all subsequent experiments were exclusively conducted with these peptides.

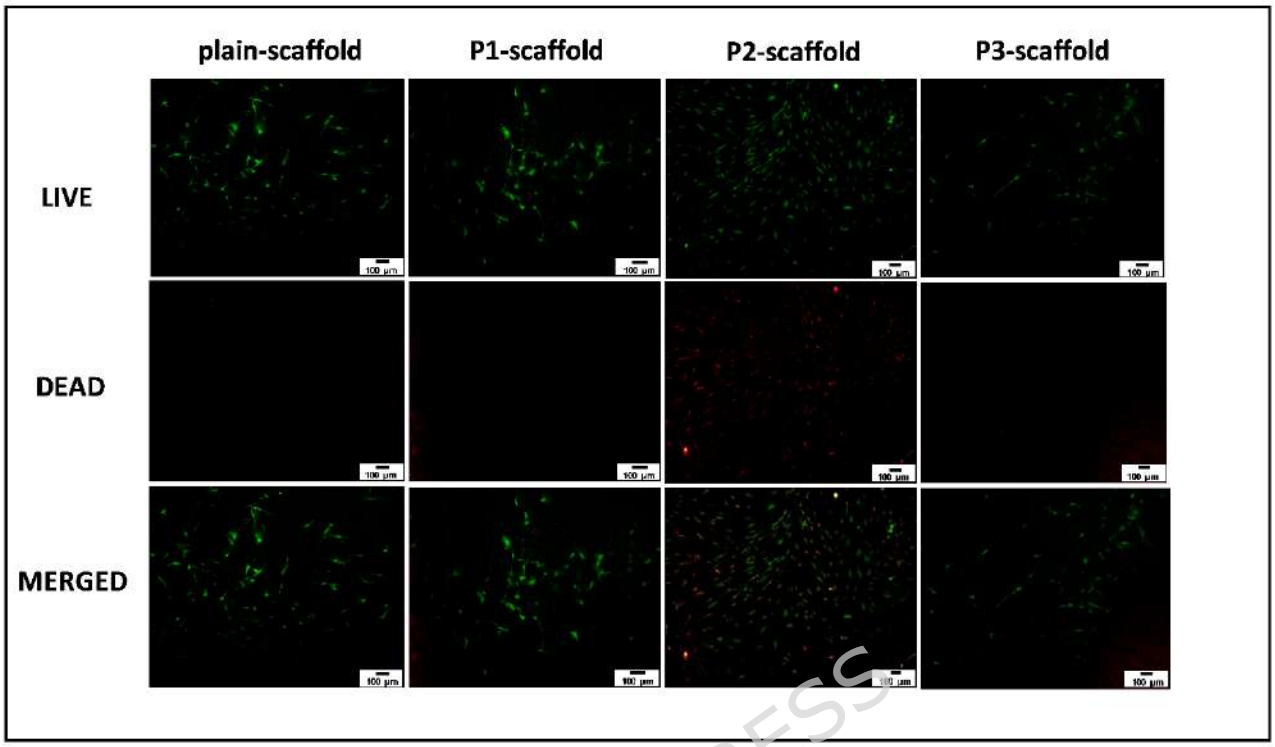

Fig. 7: Live and Dead assay on peptide-conjugated scaffolds after 72 h of incubation.

Live/dead images in Fig. 7 showed predominantly viable cells on all peptide-conjugated scaffolds and plain scaffolds after 72 h of incubation. While P1-scaffold and P3-scaffold did not display any cell death, some cell death was highlighted with P2-scaffold. In line with biocompatibility and non-toxic behavior of P2 peptide on fibroblasts for 24 h in Fig. 6, this toxicity effect may arise from time dependency or presence of toxic release products. Moreover, the observed cell death on P2-scaffold may be related to cell stress due to extensive surface moieties and cell-type selectivity, resulting in suboptimal adhesion cues for fibroblasts, since the P2 motif is known to be strongly supportive for endothelial cells. After 72 h of incubation on scaffolds, DAPI and phalloidin staining revealed extensive cell spreading and cytoskeletal organization for all scaffolds, as shown in Fig. 8. All cells exhibited well-defined actin fibers and elongated morphologies, indicating good adhesion and adaptation to the fibrous architecture.

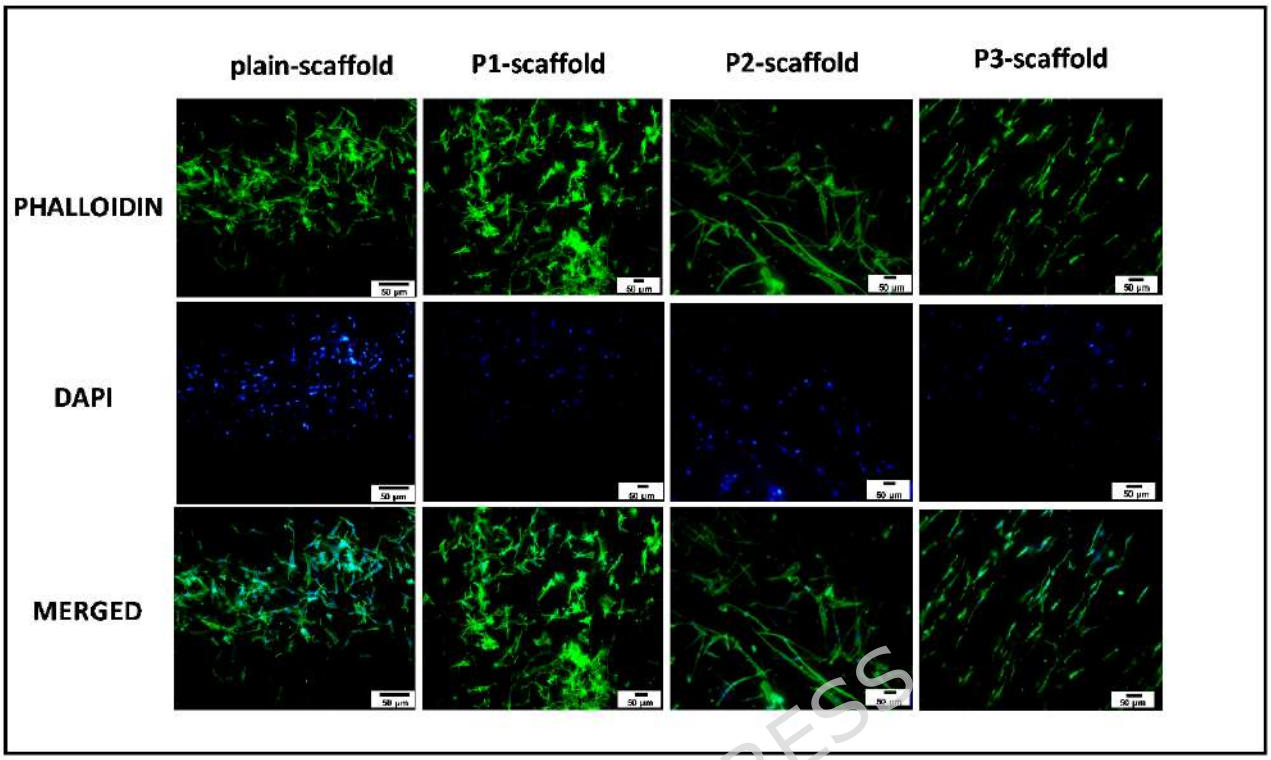

Fig. 8: DAPI and phalloidin staining on peptide-conjugated scaffolds.

3.8. Cytotoxicity and cell proliferation assessment of peptides on HUVECs

HUVECs viability after treatment with P1, P2, and P3 for 24 h and 72 h was assessed and given in Fig. 9. The cell viability results obtained at 24 h were associated with the initial cytotoxic effects of the peptides on HUVECs, whereas the results at 72 h were correlated with their effects on cell proliferation. Cell viability values above 70% were considered cytocompatible. At 24 h, P1 exhibited lower cell viability than threshold at the minimum and maximum concentrations, with values of 49% and 65%, respectively, whereas cell viability remained above 70% at intermediate concentrations. Within the first 24 h, cell viability increased as the P1 concentration increased up to 79 μM, at which maximum cell viability (157%) was observed. Further increases in P1 concentration resulted in a negative effect on cell viability, leading to a decrease. Although cell viability remained above 70% at all concentrations after 72 h, the same trend was observed at this time point. Specifically, P1 concentrations up to 79 μM promoted cell viability, whereas higher concentrations exhibited an inhibitory effect, yet still cytocompatible. An increase in cell viability was observed across all concentrations from 24 h to 72 h,

suggesting a promoting effect of P1 on HUVEC proliferation. Notably, even at concentrations that exhibited cytotoxic effects during the first 24 h, cell viability increased to within the cytocompatible range at 72 h. This suggests that, as an initial cellular response, P1 may be insufficient to promote proliferation at low concentrations, while exhibiting cytotoxic effects at higher concentrations during early exposure. However, these adverse effects were temporally tolerated by the cells and diminished over time. For P2, cell viability fell below the 70% threshold at 24 h only at the 16 μM which is the lowest concentration. Interestingly, P2 exhibited a concentration-dependent effect on HUVEC viability as well. During the first 24 h, increasing P2 concentrations enhanced cell viability up to 80 μM, whereas further increases in concentration resulted in a decrease in viability. Nevertheless, cell viability remained above the cytocompatibility threshold at higher concentrations. Unlike P1, P2 did not induce cytotoxic effects even at the highest concentration evaluated. At 72 h, cell viability increased clearly at all tested concentrations, indicating a pronounced proliferation-promoting effect. The insufficient promoting response observed at 24 h was overcome at 72 h, suggesting a time-dependent enhancement of cellular activity. Notably, the highest cell viability was consistently observed at 80 μM at both time points. P3 exhibited similar pattern on HUVECs that observed for P1. Cell viability remained below the cytocompatibility threshold only at the lowest and highest concentrations tested at 24 h. At 72 h, this effect was no longer observed, and cell viability significantly raised across all tested concentrations. Overall, P1, P2 and P3 peptide motifs demonstrated concentration-dependent biphasic cellular responses in HUVECs, characterized by enhanced cellular metabolic activity at low peptide concentrations followed by inhibitory responses at higher concentrations, which is consistent with hormetic like behavior [57]. Such biphasic responses have previously been reported [58,59] for peptides and may reflect the balance between stimulatory bioactive signaling at optimal concentrations and unfavorable cellular effects at elevated peptide exposure levels. Since integrin-mediated interactions play critical roles in endothelial cell adhesion, migration, survival, and downstream signaling pathways, elevated peptide concentrations may alter receptor-mediated signaling balance and cellular interactions [60–62]. In addition, localized physicochemical effects associated with elevated peptide concentrations, including possible osmotic

imbalance or microenvironmental changes, may also have cause the inhibitory effect on cell viability observed at higher peptide exposure levels [63,64]. In this study, P1, P2 and P3, cell viability was promoted within a certain concentration window, identified as 79, 80, and 64 μM respectively. All these concentrations correspond to 50 μg/mL of peptide in cell culture medium. This finding indicates the presence of an optimal concentration range at which the peptides effectively enhance cellular activity without inducing cytotoxic effects. Concentrations outside this range resulted in reduced cellular responses, highlighting the importance of dose optimization for achieving favorable cytocompatibility and proliferation outcomes. In addition, at higher concentrations of P3 (128 and 256 μM equals to 100 μg/mL and 200 μg/mL respectively) was observed to enhance cell proliferation in 72 h to a greater extent compared with P1 and P2 at the same concentrations, 159 and 317 μM of P1 and 161 and 322 μM of P2 which are 100 μg/mL and 200 μg/mL of peptide solution.

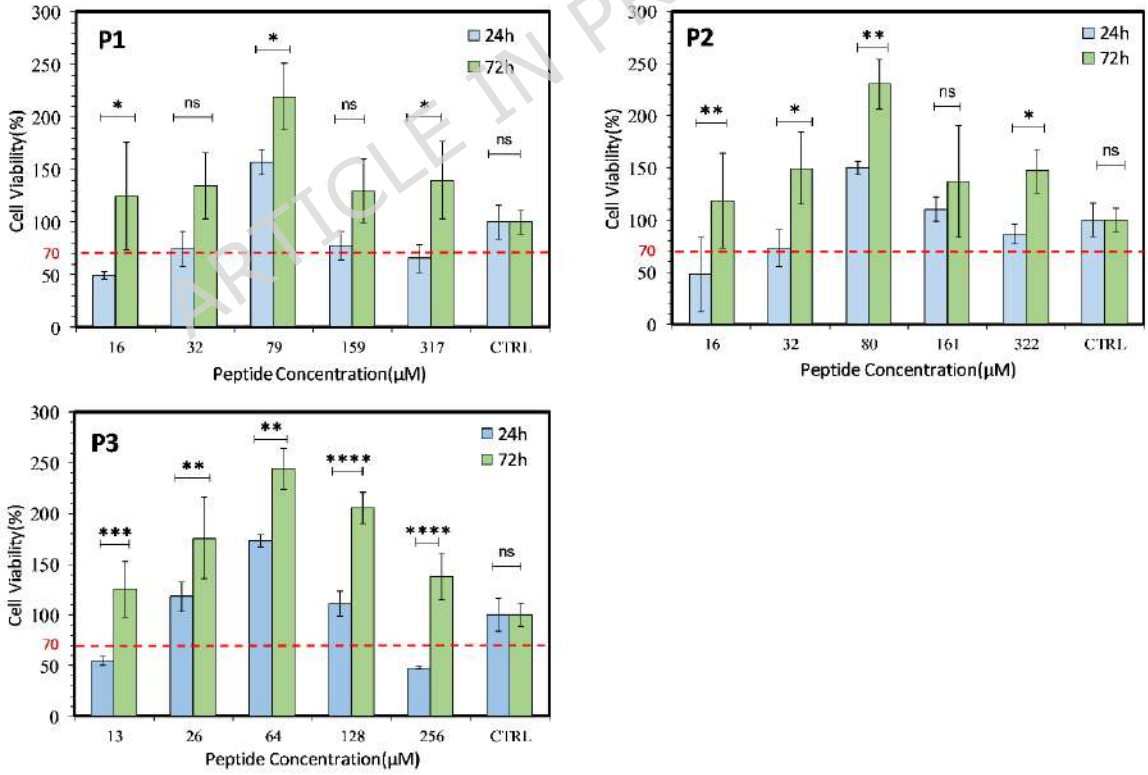

Fig. 9: HUVECs viability at 24 h and 72 h after P1, P2 and P3 treatment at varied concentrations. Statistical significance was defined as follows: ns, not significant ($p \geq 0.05$); *$p < 0.05$, significant;

**p < 0.01, very significant; ***p < 0.001, extremely significant; and ****p < 0.0001, extremely significant. Peptide concentrations were prepared at equivalent mass concentrations (μg/mL). Corresponding molar concentrations differed among peptides due to differences in molecular weight accordingly.

In comparison with cell viability was evaluated after 24 h of incubation of P1, P2, and P3 at identical concentrations for fibroblasts in Fig. 6 previously reported, endothelial cells were found to be more sensitive to the peptides and exhibited greater dose-dependent variation in their responses. For P1, cell viability in fibroblasts was higher than that in endothelial cells at most concentrations, except at 79 μM. In contrast, for P2, endothelial cells exhibited higher viability than fibroblasts at elevated concentrations, indicating a more pronounced endothelial-specific response. For P3, the highest cell viability for both cell type was observed at a concentration of 64 μM. Although endothelial cells exhibited higher viability at certain peptide concentrations during the first 24 h, fibroblasts demonstrated greater overall tolerance across all concentrations and did not experience a toxic effect. Among the peptides, P2 showed the highest compatibility with endothelial cells at higher concentrations, as it did not reduce cell viability below the threshold and showed higher viability than P1 and P3 with greatest concentration.

3.9. Cytotoxicity and cell proliferation assessment of peptide-conjugated scaffolds on HUVECs

Furthermore, the release-associated cytotoxicity and the effects of released products on cell proliferation were evaluated for P1- and P2-conjugated scaffolds which these motifs are known effective toward endothelial cells [14–16,19,22,65,66], as well as plain scaffolds. Cell viability was assessed by MTT assay at 24 h and 72 h to investigate both the short-term cytotoxic effects and the time-dependent influence of scaffold-derived release products on HUVEC proliferation. At 24 h, all scaffold extracts exhibited cell viability values above the 70% in Fig. 10. Notably, the extract derived from the plain scaffold resulted in approximately threefold higher cell viability compared with the P1- and P2-conjugated scaffold extracts. However, after 72 h of incubation, a decrease in cell viability was observed in all extract-treated groups. The P1-scaffold extract induced a pronounced reduction in metabolic activity at 72 h, inhibiting cell viability and resulting in a decrease for cell viability from 109% to 38%. In contrast, incubation with the P2-scaffold

extract for 72 h also led to a reduction in cell viability; however, this decrease was not statistically significant, and cell viability remained above the 70%. For the plain scaffold extract, although cell viability reached approximately 150% at 72 h, prolonged incubation resulted a significant inhibition of cellular metabolic activity. Based on the peptide conjugation results summarized in Table 3 previously, the amounts of peptide present in the P1- scaffolds and P2-scaffolds used for the extraction studies were calculated to be 63.36 μg and 56.4 μg, respectively. In this study, peptide release kinetics were not investigated. However, to estimate the peptide concentration present in the scaffold extracts, a complete (100%) release of the conjugated peptide into the extraction medium was assumed to find theoretical maximum exposure concentration. When a complete peptide release from scaffolds was assumed during the 3-day extraction period, the maximum peptide concentrations treated were estimated to be 33.34 μg/mL (52.8 μM) and 23.5 μg/mL (37.9 μM) for the P1- and P2-scaffold extracts, respectively. According to the cell viability assessments of these peptides on HUVECs presented in Fig. 9, within this concentration range, P1 and P2 did not exhibit cytotoxic effects on HUVECs; instead, they demonstrated a promoter effect. Although PLGA is an FDA-approved and biocompatible polymer widely used in biomedical applications, the accumulation of its degradation products, lactic acid and glycolic acid, can lead to a decrease in the local pH [67] and potentially induce adverse effects [68,69]. It has been shown that acidic by-products generated during PLGA degradation can negatively affect cell viability and proliferation [70,71]. However, it has been demonstrated that this effect is bufferable and can be mitigated [68,72]. In particular, it has been reported that PLGA-derived by-products accumulate in vascular endothelial cells, leading to oxidative stress; however, activation of molecular pathway and the expression of inflammation-related factors caused by degradation products of PLGA was shown to be effectively mitigated by the incorporation of magnesium hydroxide [73]. In the present study, the possible acidic environment induced by PLGA degradation was tolerated by cells at 24 h; however, prolonged exposure might lead to a significant reduction in cell viability at 72 h as shown in Fig. 10. As the highest viability decrease found with the plain scaffold extract, it supports that viability inhibition is consistent with the accumulation of acidic degradation by-products over time. Although the presence of P1 and P2 peptides in the extracts did not

completely prevent the cell viability reduction and cell viability in the P1-scaffold extract group decreased below 70% at 72 h, P1 and P2 peptide may have reduced the rate of decline in cellular viability and, exhibit a protective or stabilizing role during prolonged exposure to scaffold extracts relative to the plain scaffold extract. Notably, the reduction in cell viability observed with the P2-scaffold extract was not statistically significant, indicating that P2 more effectively supported the maintenance of cellular metabolic activity during prolonged extract exposure compared with P1.

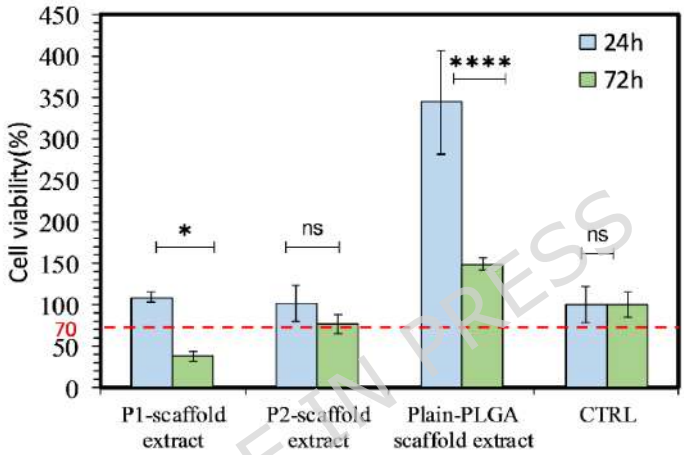

Fig. 10: HUVEC viability at 24 h and 72 h after peptide conjugated scaffold extraction treatment. Statistical significance was defined as follows: ns, not significant ($p \geq 0.05$); *$p < 0.05$, significant; **$p < 0.01$, very significant; ***$p < 0.001$, extremely significant; and ****$p < 0.0001$, extremely significant.

4. CONCLUSION

This study systematically investigated a small peptide library to establish a peptide mediated surface engineering approach for electrospun PLGA scaffolds, with a focus on physicochemical properties, biocompatibility, and endothelial cell responses. Peptide conjugation was successfully achieved through the combination of EDC/NHS coupling and thiol chemistry without compromising the structural integrity or bulk properties of the electrospun scaffolds, while tuning the surface characteristics and early endothelial cellular responses. Among the investigated motifs, P1, P2, and P3 demonstrated favorable biocompatibility and supported early endothelial cell responses by showing biphasic dose response, whereas P5 exhibited concentration-dependent cytotoxicity.

Findings highlight the importance of peptide dose optimization during scaffold surface functionalization and indicate that different peptide motifs may distinctly modulate extract-associated cellular metabolic activity during prolonged exposure, thereby affecting cellular responses in a peptide-dependent manner. Although the present work focused on early cellular responses, it contributes the future optimal dosing strategies for peptide-functionalized biomaterial surfaces intended for vascular applications such as vascular grafts, stents, and patches where endothelialization is a critical strategy for achieving antithrombogenicity. Although the present study was limited to establishing a peptide functionalization approach for electrospun scaffolds, further studies are required to evaluate long-term endothelial cell responses and hemocompatibility, as well as to mechanical assessments of tubular scaffold configurations. Since peptide conjugation may potentially alter the properties of electrospun scaffolds through changes in surface interactions, hydration behavior, and degradation characteristics, future studies involving cyclic loading, dynamic mechanical analysis (DMA), compliance, and fatigue resistance assessments would be particularly valuable for vascular graft and stent applications to better understand the long-term effects of peptide modification on mechanical performance.

CRediT authorship contribution statement: Nursu Erdogan: Conceptualization, Methodology, Investigation, Validation, Visualization, Project administration, Writing - Original Draft, Writing - Review & Editing. **Enrica Chiesa:** Methodology, Investigation, Validation, Writing - Review & Editing, Resources, Supervision. **Mariella Rosalia:** Methodology. **Dhriti Santosh Shenoy:** Methodology (peptide synthesis), Investigation (peptide synthesis and characterization); Writing - Review & Editing, **Kaliroi Peqini:** Methodology (peptide synthesis), **Sara Pellegrino:** Methodology (peptide synthesis); Writing - Review & Editing, Resources, Supervision. **Ida Genta:** Writing - Review & Editing, Resources, Supervision.

Funding: This project has received funding from the European Union's research and innovation programme under the Marie Skłodowska-Curie grant agreement no. 101072645.

Competing interest: The authors declare that they have no known competing financial interests or personal relationships that could have appeared to influence the work reported in this paper. Enrica Chiesa declares she is an Editorial Board Member of Discover Materials and confirms that she was not involved in the handling or decision-making of her own submission.

Acknowledgement: Prof. G. Bruni (Chemistry Department, University of Pavia) and Dr. A. Girella (CISRiC - Arvedi lab, University of Pavia) are acknowledged for SEM analyses.

Appendix A. Supplementary information: Supplementary data to this article can be found online.

Data Availability Statement: Work data were deposited into the Nanoremedi-UNIPV repository and are available at the following URL:
https://doi.org/10.13130/RD_UNIMI/5M4EOZ

https://doi.org/10.13130/RD_UNIMI/LS2TQM

Declarations:

Ethical approval: Ethical approval was not required for this study since human participants or animal experiments were not involved.

Consent to participate: Not applicable.

Consent to publish: Not applicable.

REFERENCES

1. Ratner BD, Zhang G. A History of Biomaterials. In: *Biomaterials Science*. Elsevier; 2020:21-34. doi:10.1016/B978-0-12-816137-1.00002-7

2. Baskaran P, Muthiah B, Uthirapathy V. A systematic review on biomaterials and their recent progress in biomedical applications: bone tissue engineering. *Reviews in Inorganic Chemistry*. 2025;45(4):747-781. doi:10.1515/revic-2024-0062

3. Chakrapani G, Vijay Kumar V, Zare M. Next-Generation Biomaterials: Design Strategies, Clinical Translation, and the Rise of Intelligent Therapeutic Platforms. *ACS Omega*. 2025;10(40):46272-46293. doi:10.1021/acsomega.5c06034

4. Hench LL, Polak JM. Third-Generation Biomedical Materials. *Science*. 2002;295(5557):1014-1017. doi:10.1126/science.1067404

5. Lang Z, Chen T, Zhu S, et al. Construction of vascular grafts based on tissue-engineered scaffolds. *Materials Today Bio*. 2024;29:101336. doi:10.1016/j.mtbio.2024.101336

6. Wang N, Chen J, Hu Q, et al. Small diameter vascular grafts: progress on electrospinning matrix/stem cell blending approach. *Front Bioeng Biotechnol*. 2024;12:1385032. doi:10.3389/fbioe.2024.1385032

7. Yalcin Enis I, Gok Sadikoglu T. Design parameters for electrospun biodegradable vascular grafts. *Journal of Industrial Textiles*. 2018;47(8):2205-2227. doi:10.1177/1528083716654470

8. Nitti P, Narayanan A, Pellegrino R, Villani S, Madaghiele M, Demitri C. Cell-Tissue Interaction: The Biomimetic Approach to Design Tissue Engineered Biomaterials. *Bioengineering*. 2023;10(10):1122. doi:10.3390/bioengineering10101122

9. Ravindran S, Gao Q, Kotecha M, et al. Biomimetic Extracellular Matrix-Incorporated Scaffold Induces Osteogenic Gene Expression in Human Marrow Stromal Cells. *Tissue Engineering Part A*. 2012;18(3-4):295-309. doi:10.1089/ten.tea.2011.0136

10. Hao D, Swindell HS, Ramasubramanian L, et al. Extracellular Matrix Mimicking Nanofibrous Scaffolds Modified With Mesenchymal Stem Cell-Derived Extracellular Vesicles for Improved Vascularization. *Front Bioeng Biotechnol*. 2020;8:633. doi:10.3389/fbioe.2020.00633

11. Tallawi M, Rosellini E, Barbani N, et al. Strategies for the chemical and biological functionalization of scaffolds for cardiac tissue engineering: a review. *J R Soc Interface*. 2015;12(108):20150254. doi:10.1098/rsif.2015.0254

12. Xia D, Chen J, Zhang Z, Dong M. Emerging polymeric biomaterials and manufacturing techniques in regenerative medicine. *Aggregate*. 2022;3(5):e176. doi:10.1002/agt2.176

13. Rickel AP, Deng X, Engebretson D, Hong Z. Electrospun nanofiber scaffold for vascular tissue engineering. *Materials Science and Engineering: C*. 2021;129:112373. doi:10.1016/j.msec.2021.112373

14. Onak Pulat G, Tatar AG, Usta YH, Karaman O. Improved endothelial cell proliferation on laminin-derived peptide conjugated nanofibrous microtubes using custom made bioreactor. *International Advanced Researches and Engineering Journal*. 2022;6(3):220-226. doi:10.35860/iarej.1096616

15. Asakura T, Hayashi T, Tanaka T, Tatematsu K ichiro, Sezutsu H. Promotion of endothelialization of silk functionalized with IKVAV peptide and production of silk containing IKVAV-REDV sequence by transgenic silkworms. *J Biomater Appl*. 2025;40(3):402-418. doi:10.1177/08853282251345003

16. Grant DS, Kinsella JL, Fridman R, et al. Interaction of endothelial cells with a laminin A chain peptide (SIKVAV) in vitro and induction of angiogenic behavior in vivo. *Journal Cellular Physiology*. 1992;153(3):614-625. doi:10.1002/jcp.1041530324

17. Chen S, Zhang M, Shao X, et al. A laminin mimetic peptide SIKVAV-conjugated chitosan hydrogel promoting wound healing by enhancing angiogenesis, re-epithelialization and collagen deposition. *J Mater Chem B*. 2015;3(33):6798-6804. doi:10.1039/C5TB00842E

18. Song Y, Li Y, Zheng Q. Angiogenesis induced by IKVAV-Containing amphiphile peptide in vivo. *J Wuhan Univ Technol-Mat Sci Edit*. 2010;25(5):803-806. doi:10.1007/s11595-010-0096-x

19. Asakura T, Shimokawatoko H, Nakazawa Y. Characterization and promotion of endothelialization of Bombyx mori silk fibroin functionalized with REDV peptide. *International Journal of Biological Macromolecules*. 2024;261:129746. doi:10.1016/j.ijbiomac.2024.129746

20. Mahara A, Li M, Ohya Y, Yamaoka T. Small-Diameter Synthetic Vascular Graft Immobilized with the REDV Peptide Reduces Early-Stage Fibrin Clot Deposition and Results in Graft Patency in Rats. *Biomacromolecules*. 2020;21(8):3092-3101. doi:10.1021/acs.biomac.0c00457

21. Zhou J, Wang M, Wei T, et al. Endothelial Cell-Mediated Gene Delivery for In Situ Accelerated Endothelialization of a Vascular Graft. *ACS Appl Mater Interfaces*. 2021;13(14):16097-16105. doi:10.1021/acsami.1c01869

22. Ohya Y, Nishimura K, Sumida H, et al. Cellular attachment behavior on biodegradable polymer surface immobilizing endothelial cell-specific peptide. *Journal of Biomaterials Science, Polymer Edition*. 2020;31(11):1475-1488. doi:10.1080/09205063.2020.1762325

23. Malcor JD, Hunter EJ, Davidenko N, et al. Collagen scaffolds functionalized with triple-helical peptides support 3D HUVEC culture. *Regenerative Biomaterials*. 2020;7(5):471-482. doi:10.1093/rb/rbaa025

24. Reyes CD, García AJ. Engineering integrin-specific surfaces with a triple-helical collagen-mimetic peptide. *J Biomedical Materials Res*. 2003;65A(4):511-523. doi:10.1002/jbm.a.10550

25. Ichise SF, Takeuchi S, Aoki S, et al. Development of a collagen-like peptide polymer via end-to-end disulfide cross-linking and its application as a biomaterial. *Acta Biomaterialia*. 2019;94:361-371. doi:10.1016/j.actbio.2019.06.010

26. Turner KR, Adams C, Staelens S, Deckmyn H, San Antonio J. Crucial Role for Endothelial Cell α2β1 Integrin Receptor Clustering in Collagen-Induced Angiogenesis. *The Anatomical Record*. 2020;303(6):1604-1618. doi:10.1002/ar.24277

27. García JR, Clark AY, García AJ. Integrin-specific hydrogels functionalized with VEGF for vascularization and bone regeneration of critical-size bone defects. *J Biomedical Materials Res*. 2016;104(4):889-900. doi:10.1002/jbm.a.35626

28. Mansour A, Darwiche W, Yaker L, et al. GFOGER Peptide Modifies the Protein Content of Extracellular Vesicles and Inhibits Vascular Calcification. *Front Cell Dev Biol*. 2020;8:589761. doi:10.3389/fcell.2020.589761

29. Shammas NW. Bivalirudin: Pharmacology and Clinical Applications. *Cardiovascular Drug Reviews*. 2006;23(4):345-360. doi:10.1111/j.1527-3466.2005.tb00177.x

30. Sun Q, Si J, Zhao L, et al. Direct thrombin inhibitor-bivalirudin improved the hemocompatibility of electrospun polycaprolactone vascular grafts. *Composites Part B: Engineering*. 2022;234:109702. doi:10.1016/j.compositesb.2022.109702

31. Yang Z, Tu Q, Maitz MF, Zhou S, Wang J, Huang N. Direct thrombin inhibitor-bivalirudin functionalized plasma polymerized allylamine coating for improved biocompatibility of vascular devices. *Biomaterials*. 2012;33(32):7959-7971. doi:10.1016/j.biomaterials.2012.07.050

32. Nomizu M, Kuratomi Y, Song SY, et al. Identification of Cell Binding Sequences in Mouse Laminin γ1 Chain by Systematic Peptide Screening. *Journal of Biological Chemistry*. 1997;272(51):32198-32205. doi:10.1074/jbc.272.51.32198

33. Ponce ML, Nomizu M, Kleinman HK. An angiogenic laminin site and its antagonist bind through the αvβ3 and α5β1 integrins. *The FASEB Journal*. 2001;15(8):1389-1397. doi:10.1096/fj.00-0736com

34. Chen H, Fu X, Jiang J, Han S. C16 Peptide Promotes Vascular Growth and Reduces Inflammation in a Neuromyelitis Optica Model. *Front Pharmacol*. 2019;10:1373. doi:10.3389/fphar.2019.01373

35. Malinda KM, Wysocki AB, Koblinski JE, Kleinman HK, Ponce ML. Angiogenic laminin-derived peptides stimulate wound healing. *The International Journal of Biochemistry & Cell Biology*. 2008;40(12):2771-2780. doi:10.1016/j.biocel.2008.05.025

36. Zachman AL, Crowder SW, Ortiz O, et al. Pro-angiogenic and Anti-inflammatory Regulation by Functional Peptides Loaded in Polymeric Implants for Soft Tissue Regeneration. *Tissue Engineering Part A*. 2013;19(3-4):437-447. doi:10.1089/ten.tea.2012.0158

37. Zachman AL, Wang X, Tucker-Schwartz JM, et al. Uncoupling angiogenesis and inflammation in peripheral artery disease with therapeutic peptide-loaded microgels. *Biomaterials*. 2014;35(36):9635-9648. doi:10.1016/j.biomaterials.2014.08.011

38. Bucci R, Vaghi F, Erba E, Romanelli A, Gelmi ML, Clerici F. Peptide grafting strategies before and after electrospinning of nanofibers. *Acta Biomaterialia*. 2021;122:82-100. doi:10.1016/j.actbio.2020.11.051

39. Barbosa M, Martins M, Gomes P. Grafting Techniques towards Production of Peptide-Tethered Hydrogels, a Novel Class of Materials with Biomedical Interest. *Gels*. 2015;1(2):194-218. doi:10.3390/gels1020194

40. Song DW, Kim SH, Kim HH, Lee KH, Ki CS, Park YH. Multi-biofunction of antimicrobial peptide-immobilized silk fibroin nanofiber membrane: Implications for wound healing. *Acta Biomaterialia*. 2016;39:146-155. doi:10.1016/j.actbio.2016.05.008

41. Peqini K, Attanasio S, Feni L, Cappelletti G, Pellegrino S. Breaking down and building up alpha-synuclein: An insight on its N-terminal domain. *Journal of Peptide Science*. 2024;30(4):e3556. doi:10.1002/psc.3556

42. Schneider CA, Rasband WS, Eliceiri KW. NIH Image to ImageJ: 25 years of image analysis. *Nat Methods*. 2012;9(7):671-675. doi:10.1038/nmeth.2089

43. Giglio A, Chiesa E, Iamele L, et al. Engineering anti-c-MET scFv-conjugated PLGA nanoparticles for precision verteporfin delivery in lung cancer cells: a formulation study. *International Journal of Pharmaceutics*. 2025;683:126004. doi:10.1016/j.ijpharm.2025.126004

44. LIVE/DEAD Cell Imaging Kit (488/570) - IT. Accessed December 17, 2025. https://www.thermofisher.com/uk/en/home/references/protocols/cell-and-tissue-analysis/protocols/live-dead-cell-imaging-kit-488-570.html

45. DAPI Counterstaining Protocols - IT. Accessed January 8, 2026. https://www.thermofisher.com/uk/en/home/references/protocols/cell-and-tissue-analysis/dapi-protocol/basic-dapi-counterstaining-protocols.html

46. Actin Staining Protocol - IT. Accessed January 8, 2026. https://www.thermofisher.com/uk/en/home/references/protocols/cell-and-tissue-analysis/microscopy-protocol/actin-staining-protocol.html

47. Pouroutzidou GK, Lazaridou M, Papoulia C, et al. Electrospun PLGA Membranes with Incorporated Moxifloxacin-Loaded Silica-Based Mesoporous Nanocarriers for Periodontal Regeneration. *Nanomaterials*. 2022;12(5):850. doi:10.3390/nano12050850

48. Wang B, Lu G, Song K, et al. PLGA-based electrospun nanofibers loaded with dual bioactive agent loaded scaffold as a potential wound dressing material. *Colloids and Surfaces B: Biointerfaces*. 2023;231:113570. doi:10.1016/j.colsurfb.2023.113570

49. Badaraev AD, Sidelev DV, Yurjev YN, Bukal VR, Tverdokhlebov SI. Modes development of PLGA scaffolds modification by magnetron co-sputtering of Cu and Ti targets. *J Phys: Conf Ser*. 2021;1799(1):012001. doi:10.1088/1742-6596/1799/1/012001

50. Sadeghi AR, Nokhasteh S, Molavi AM, Khorsand-Ghayeni M, Naderi-Meshkin H, Mahdizadeh A. Surface modification of electrospun PLGA scaffold with collagen for bioengineered skin substitutes. *Materials Science and Engineering: C*. 2016;66:130-137. doi:10.1016/j.msec.2016.04.073

51. Zhou C, Su S, Fan J, Lin J, Wang X. Engineered electrospun poly(lactic-co-glycolic acid)/Si3N4 nanofiber scaffold promotes osteogenesis of mesenchymal stem cell. *Front Mater*. 2022;9:991018. doi:10.3389/fmats.2022.991018

52. Duan G, Smith VH, Weaver DF. Characterization of aromatic-thiol π-type hydrogen bonding and phenylalanine-cysteine side chain interactions through *ab initio* calculations and protein database analyses. *Molecular Physics*. 2001;99(19):1689-1699. doi:10.1080/00268970110063917

53. Campos DM, Gritsch K, Salles V, Attik GN, Grosgogeat B. Surface Entrapment of Fibronectin on Electrospun PLGA Scaffolds for Periodontal Tissue Engineering. *BioResearch Open Access*. 2014;3(3):117-126. doi:10.1089/biores.2014.0015

54. Ponce ML, Nomizu M, Delgado MC, et al. Identification of Endothelial Cell Binding Sites on the Laminin γ1 Chain. *Circulation Research*. 1999;84(6):688-694. doi:10.1161/01.RES.84.6.688

55. Trinidad-Calderón PA, Varela-Chinchilla CD, García-Lara S. Natural Peptides Inducing Cancer Cell Death: Mechanisms and Properties of Specific Candidates for Cancer Therapeutics. *Molecules*. 2021;26(24):7453. doi:10.3390/molecules26247453

56. Strömstedt AA, Ringstad L, Schmidtchen A, Malmsten M. Interaction between amphiphilic peptides and phospholipid membranes. *Current Opinion in Colloid & Interface Science*. 2010;15(6):467-478. doi:10.1016/j.cocis.2010.05.006

57. Calabrese EJ. Biphasic dose responses in biology, toxicology and medicine: Accounting for their generalizability and quantitative features. *Environmental Pollution*. 2013;182:452-460. doi:10.1016/j.envpol.2013.07.046

58. Calabrese EJ. Amyloid β-Peptide: Biphasic Dose Responses. *Critical Reviews in Toxicology*. 2001;31(4-5):605-606. doi:10.1080/20014091111857

59. Calabrese EJ, Baldwin LA. Peptides and Hormesis. *Critical Reviews in Toxicology*. 2003;33(3-4):355-405. doi:10.1080/713611042

60. Short SM, Talbott GA, Juliano RL. Integrin-mediated Signaling Events in Human Endothelial Cells. Brugge J, ed. *MBoC*. 1998;9(8):1969-1980. doi:10.1091/mbc.9.8.1969

61. Le Saux G, Magenau A, Gunaratnam K, et al. Spacing of Integrin Ligands Influences Signal Transduction in Endothelial Cells. *Biophysical Journal*. 2011;101(4):764-773. doi:10.1016/j.bpj.2011.06.064

62. Birukova AA, Lee S, Starosta V, et al. A Role for VEGFR2 Activation in Endothelial Responses Caused by Barrier Disruptive OxPAPC Concentrations. Gottardi C, ed. *PLoS ONE*. 2012;7(1):e30957. doi:10.1371/journal.pone.0030957

63. Stears RL, Gullans SR. Transcriptional response to hyperosmotic stress. In: *Cell and Molecular Response to Stress*. Vol 1. Elsevier; 2000:129-139. doi:10.1016/S1568-1254(00)80012-1

64. Thiemicke A, Neuert G. Kinetics of osmotic stress regulate a cell fate switch of cell survival. *Sci Adv*. 2021;7(8):eabe1122. doi:10.1126/sciadv.abe1122

65. Hubbell JA, Massia SP, Desai NP, Drumheller PD. Endothelial Cell-Selective Materials for Tissue Engineering in the Vascular Graft Via a New Receptor. *Nat Biotechnol*. 1991;9(6):568-572. doi:10.1038/nbt0691-568

66. Zheng PX, Yu Z, Duan L, Zhang JH, Fu R, Jiang R. Covalent Immobilization of REDV Peptide on Heparin Coating Promotes Selective Adhesion of Endothelial Cells. *AMR*. 2022;1173:85-89. doi:10.4028/p-0tpt06

67. Fu K, Pack DW, Klibanov AM, Langer R. Visual Evidence of Acidic Environment Within Degrading Poly(lactic-co-glycolic acid) (PLGA) Microspheres. *Pharm Res*. 2000;17(1):100-106. doi:10.1023/A:1007582911958

68. Ji W, Yang F, Seyednejad H, et al. Biocompatibility and degradation characteristics of PLGA-based electrospun nanofibrous scaffolds with nanoapatite incorporation. *Biomaterials*. 2012;33(28):6604-6614. doi:10.1016/j.biomaterials.2012.06.018

69. Rhee S, Lee SJ. Effect of acidic degradation products of poly(lactic- *co* -glycolic)acid on the apatite-forming ability of poly(lactic- *co* -glycolic)acid-siloxane nanohybrid material. *J Biomedical Materials Res*. 2007;83A(3):799-805. doi:10.1002/jbm.a.31405

70. Meyer F, Wardale J, Best S, Cameron R, Rushton N, Brooks R. Effects of lactic acid and glycolic acid on human osteoblasts: A way to understand PLGA involvement in PLGA/calcium phosphate composite failure. *Journal Orthopaedic Research*. 2012;30(6):864-871. doi:10.1002/jor.22019

71. Sung HJ, Meredith C, Johnson C, Galis ZS. The effect of scaffold degradation rate on three-dimensional cell growth and angiogenesis. *Biomaterials*. 2004;25(26):5735-5742. doi:10.1016/j.biomaterials.2004.01.066

72. El Khatib M, Russo V, Prencipe G, et al. Amniotic Epithelial Stem Cells Counteract Acidic Degradation By-Products of Electrospun PLGA Scaffold by Improving Their Immunomodulatory Profile In Vitro. *Cells*. 2021;10(11):3221. doi:10.3390/cells10113221

73. Ko KW, Choi B, Kang EY, Shin SW, Baek SW, Han DK. The antagonistic effect of magnesium hydroxide particles on vascular endothelial activation induced by acidic PLGA degradation products. *Biomater Sci*. 2021;9(3):892-907. doi:10.1039/D0BM01656J

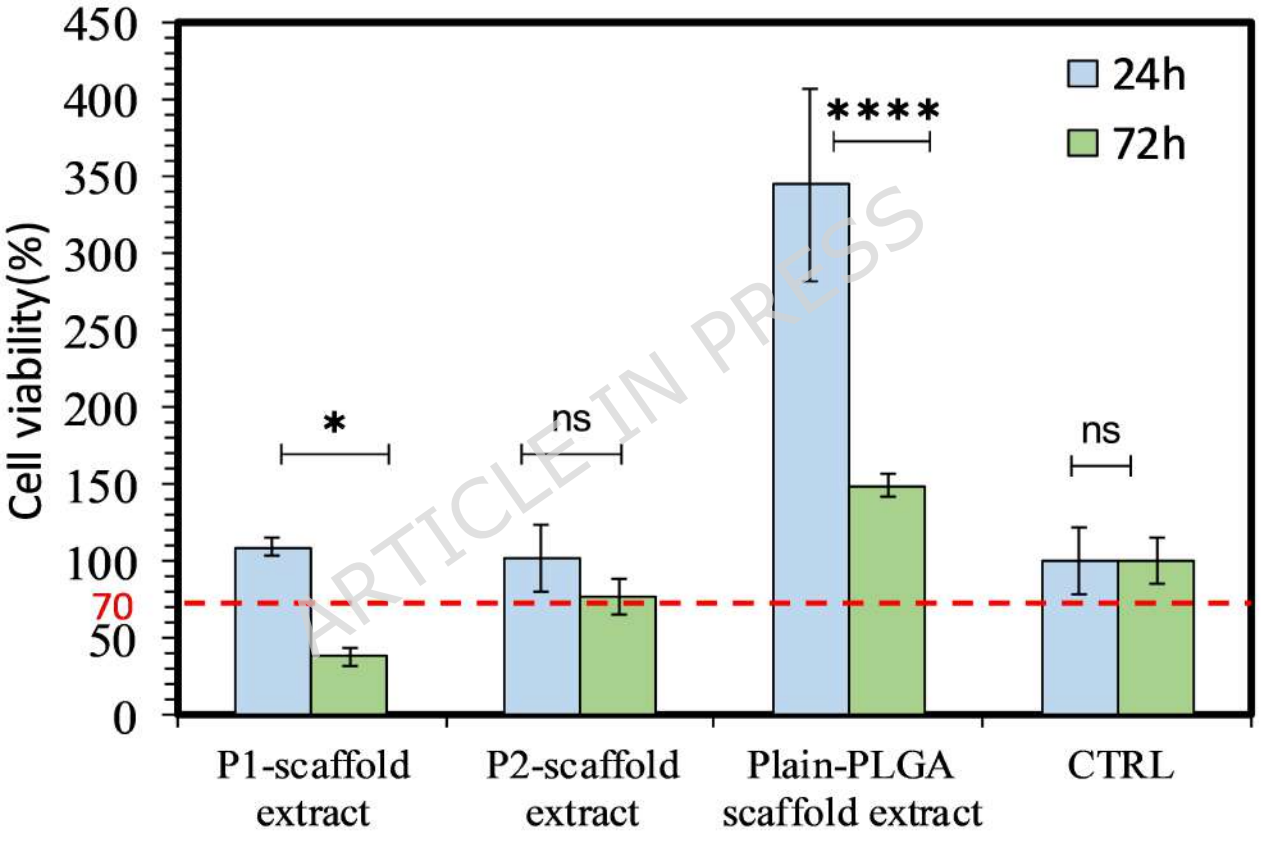

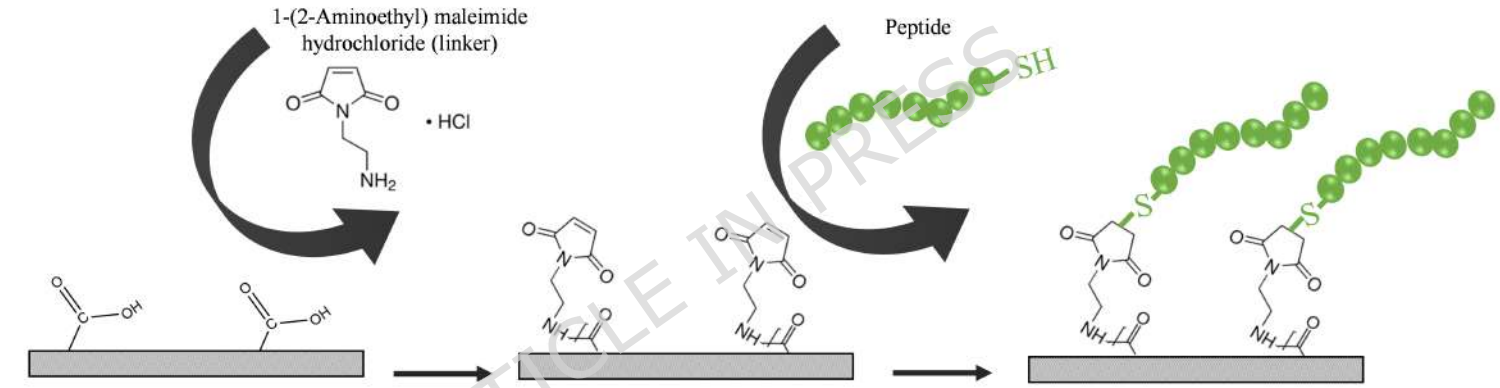

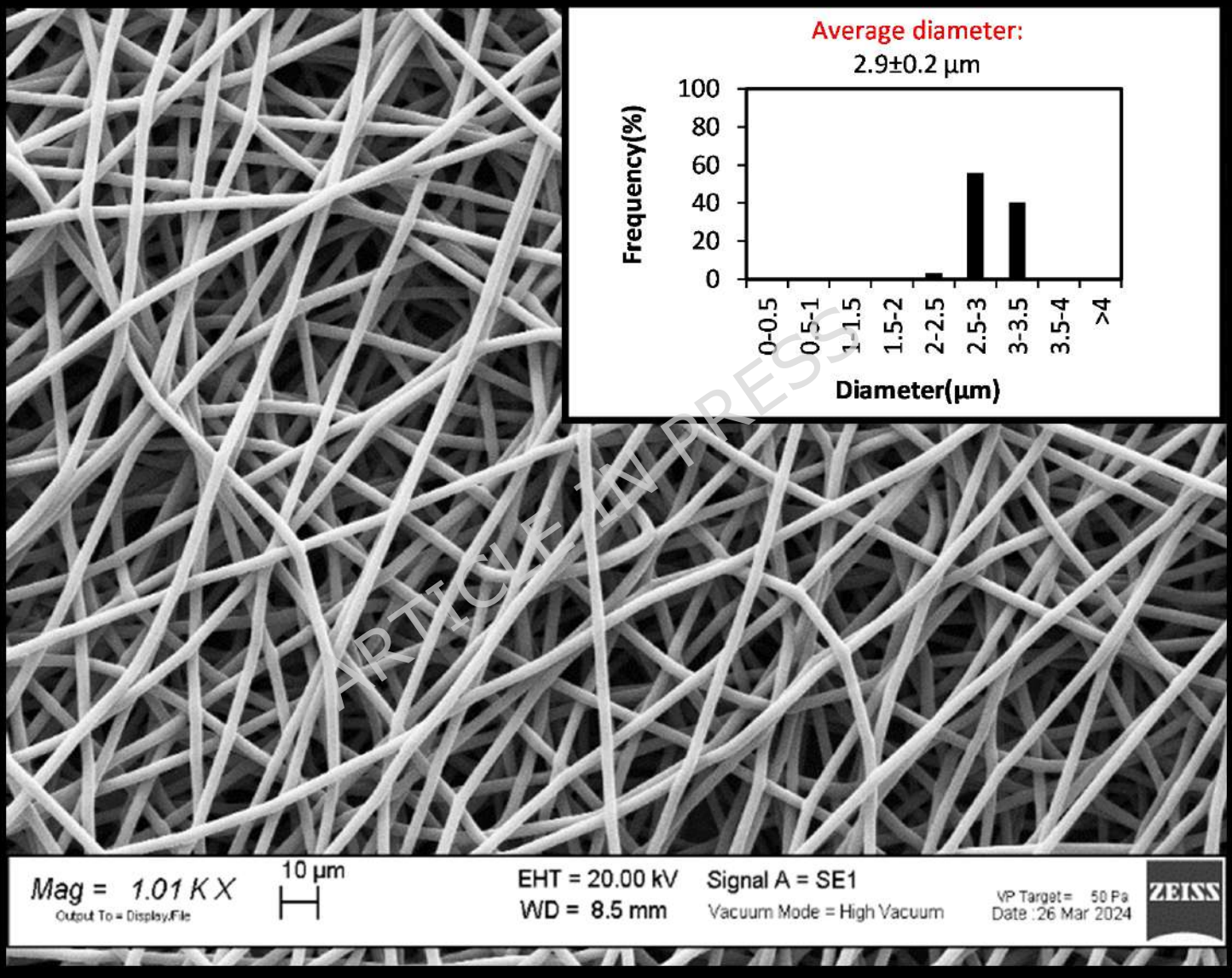

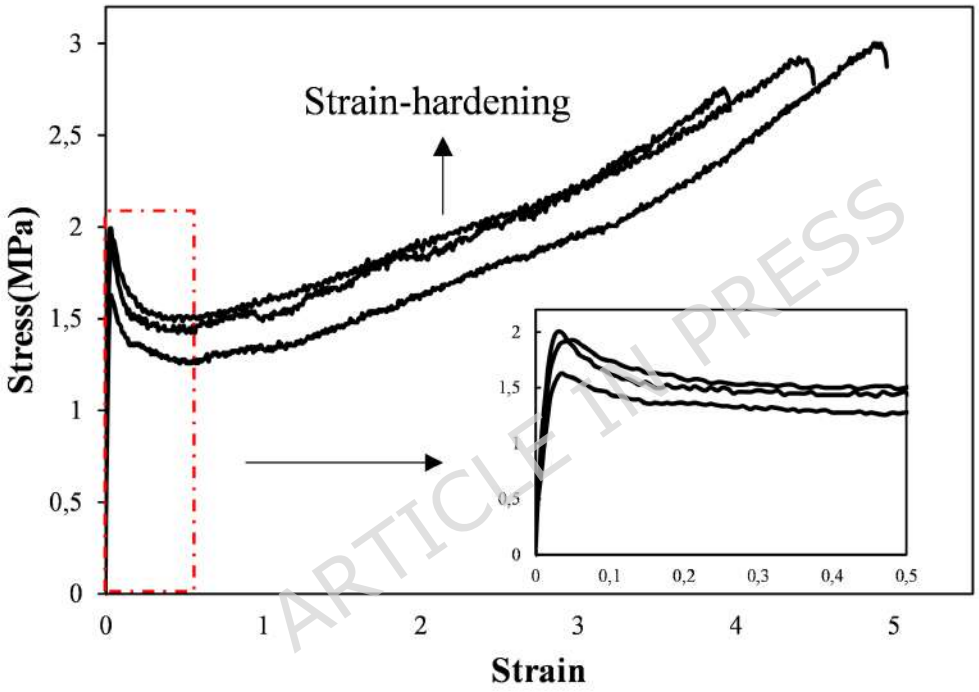

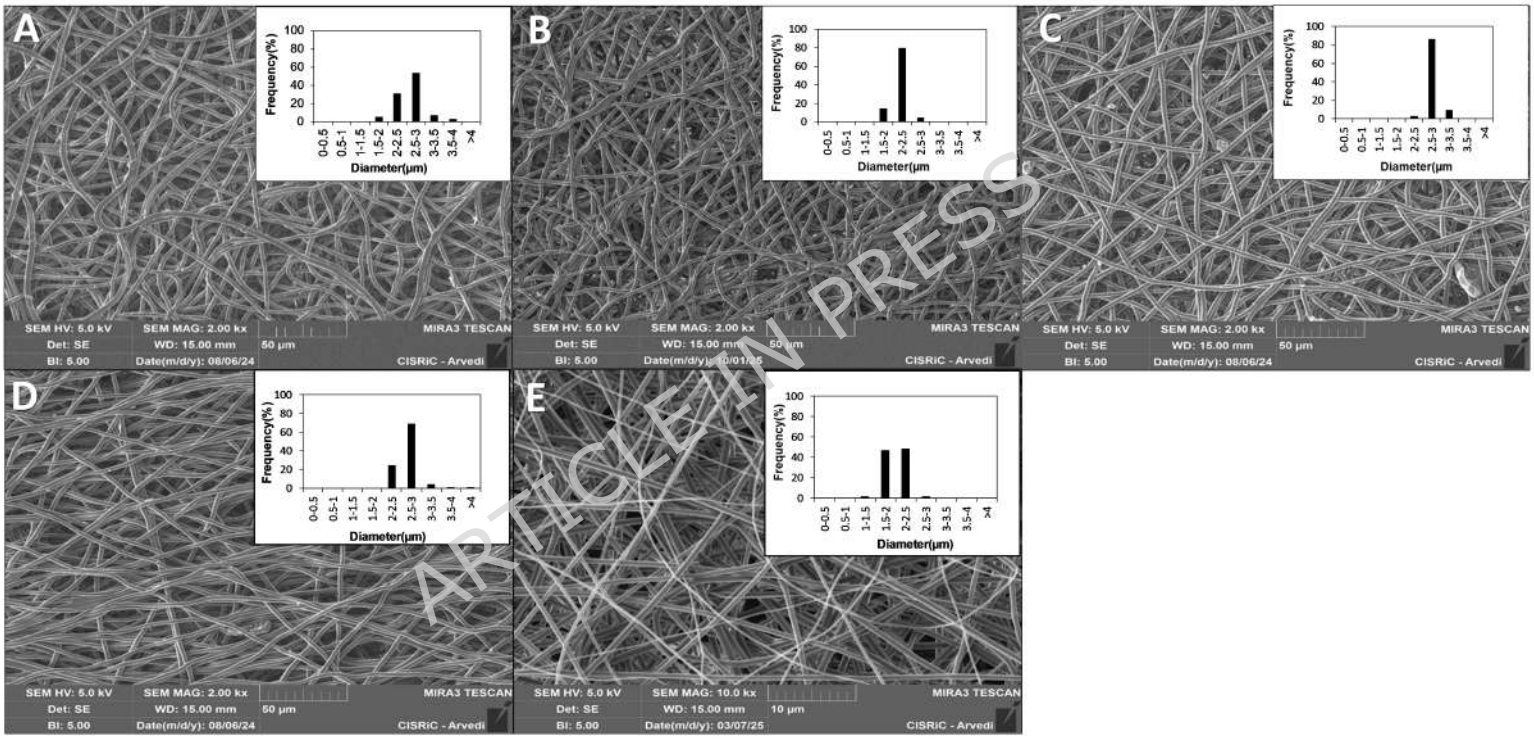

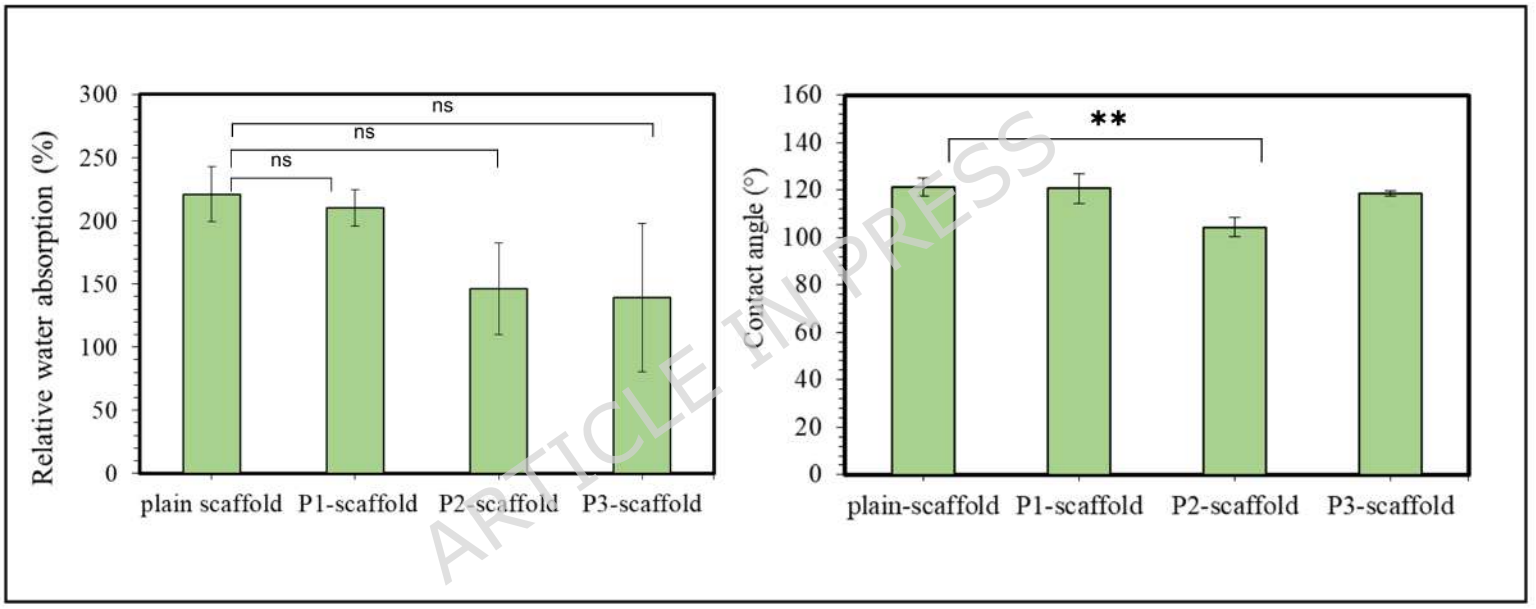

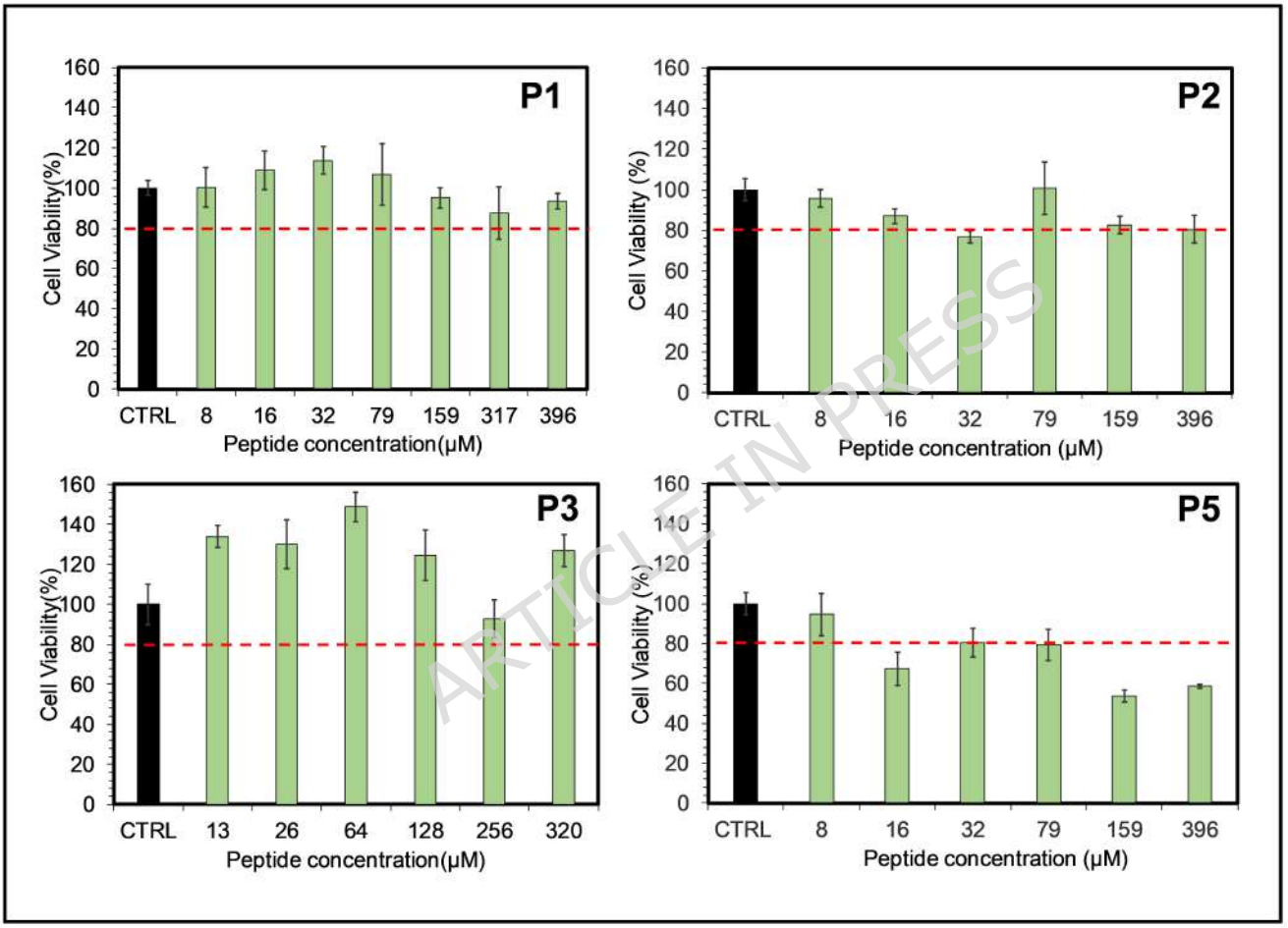

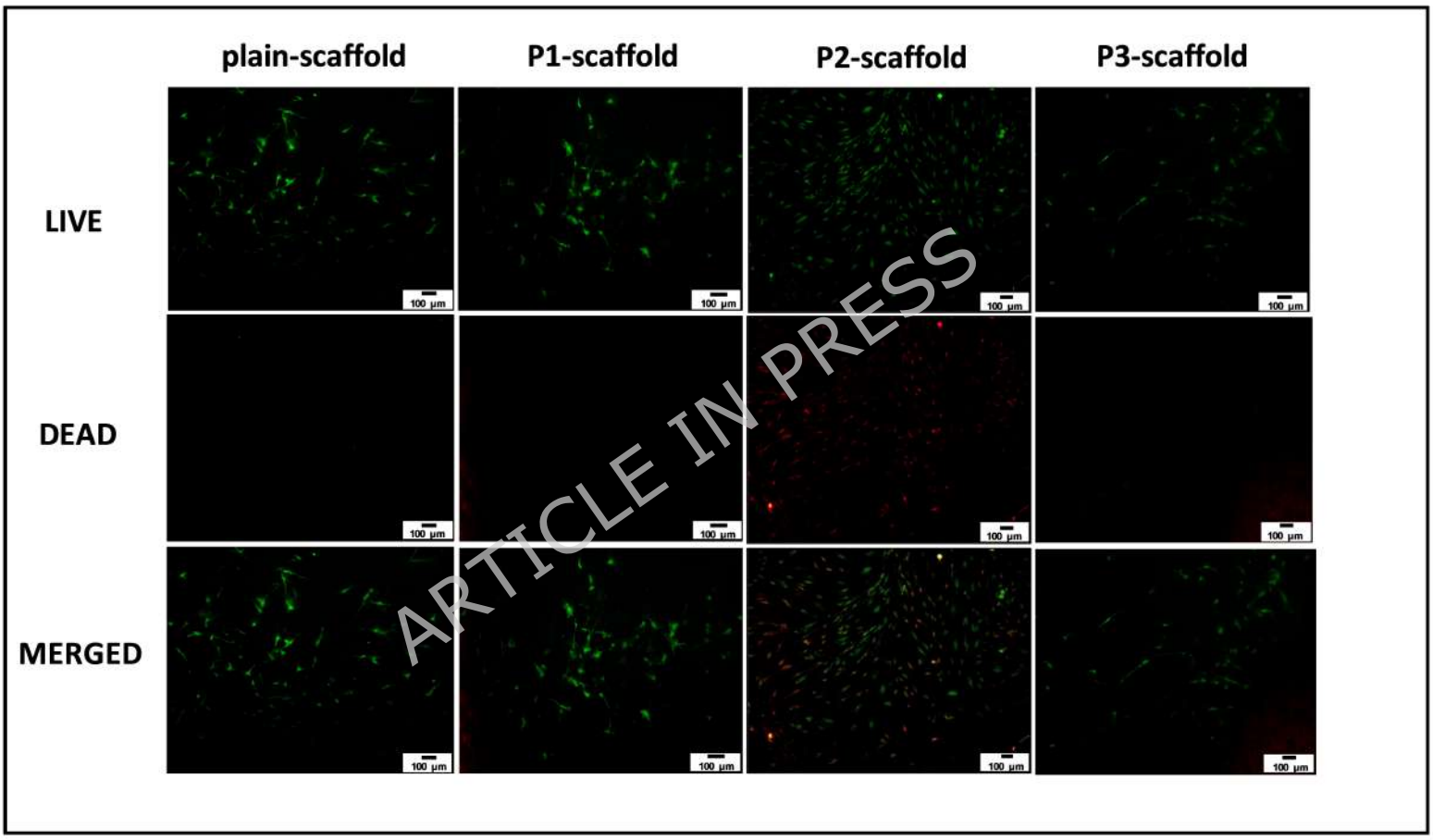

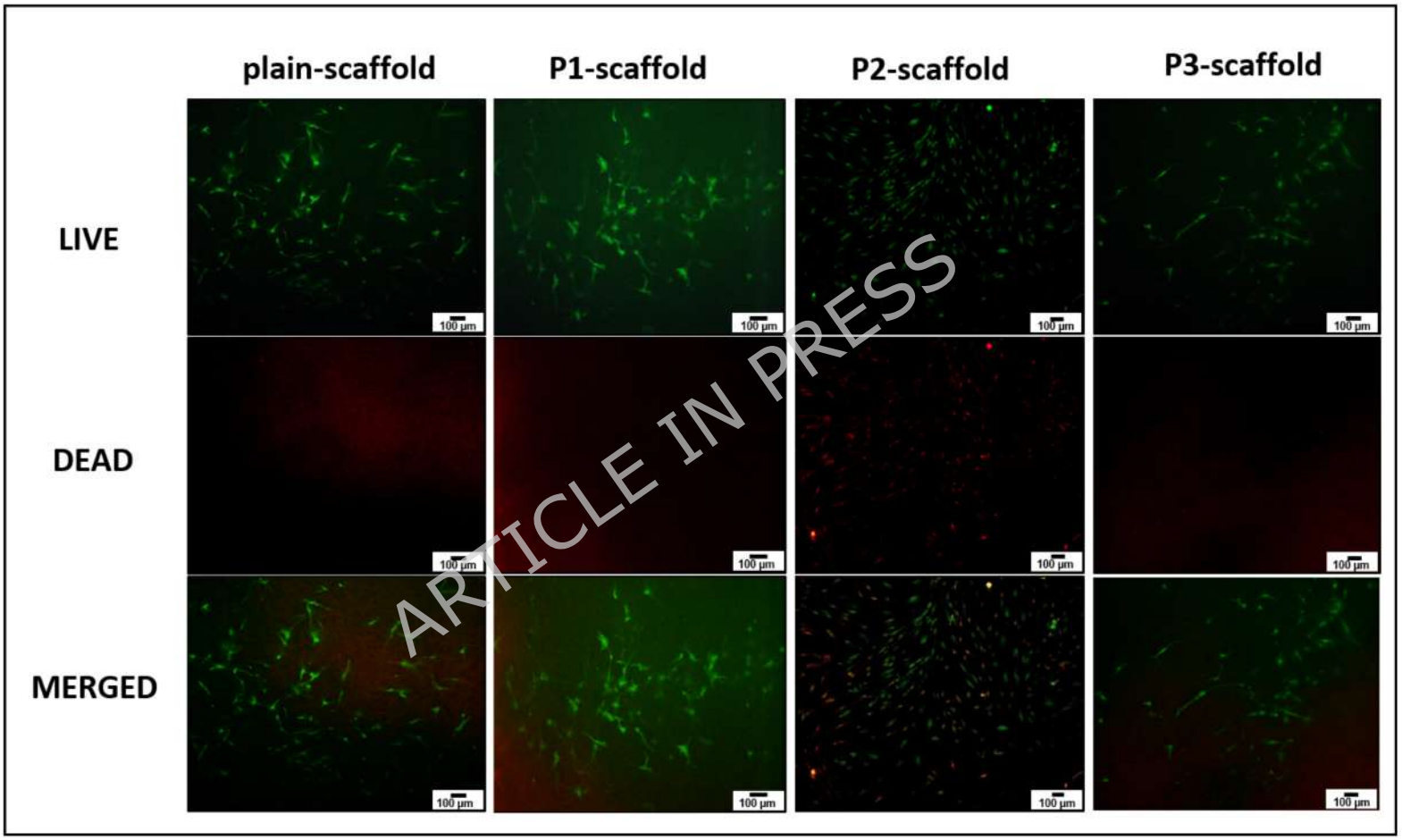

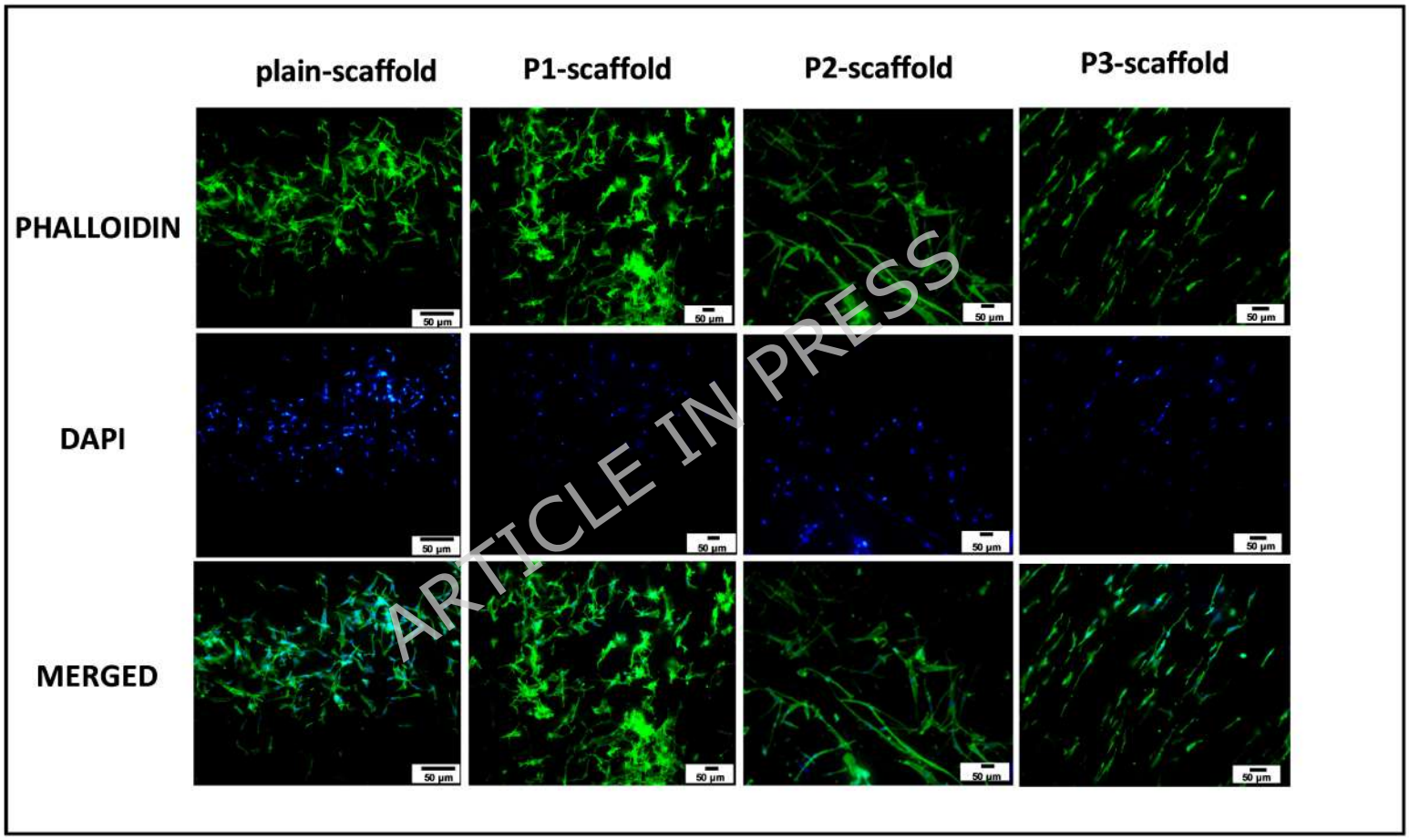

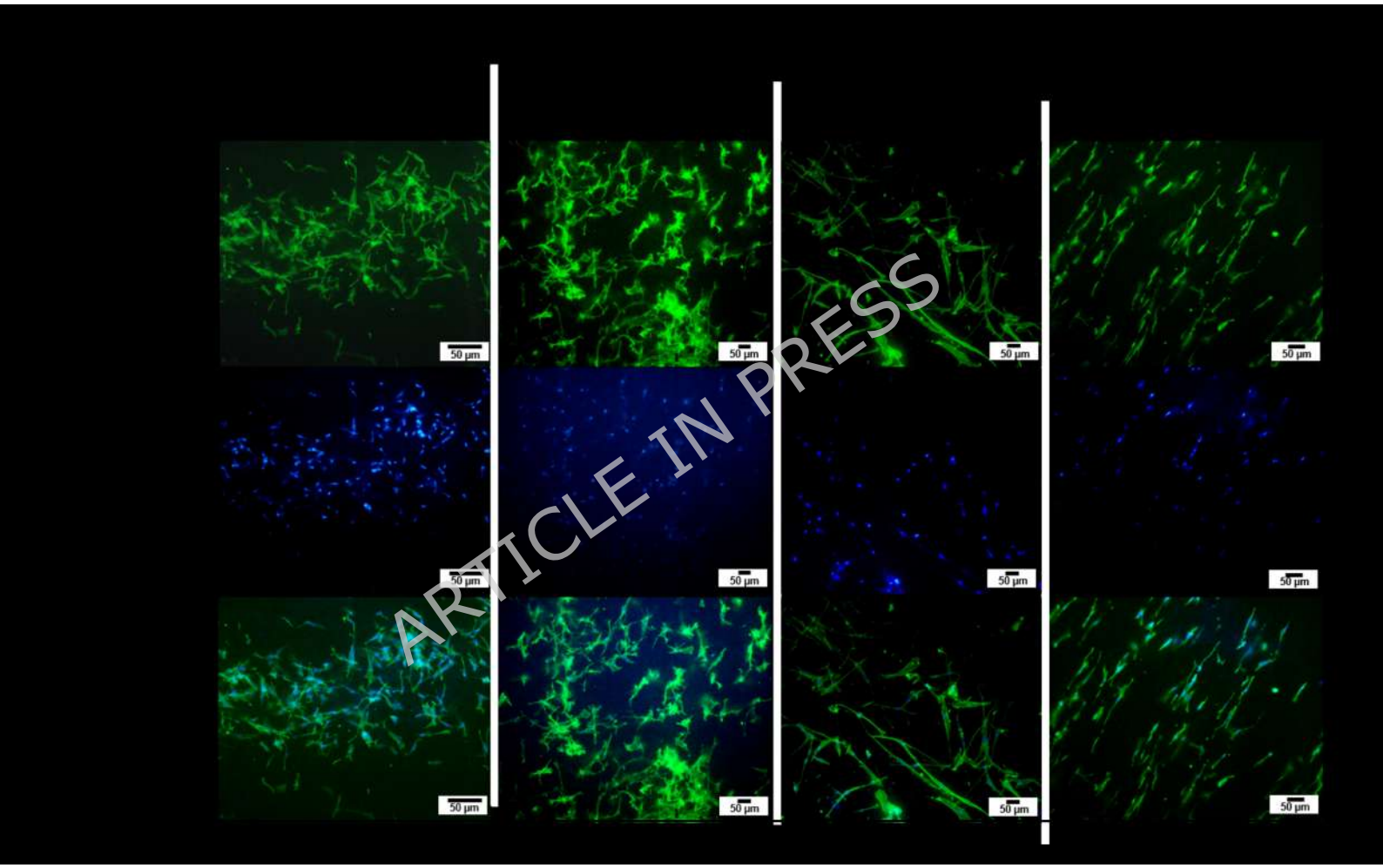

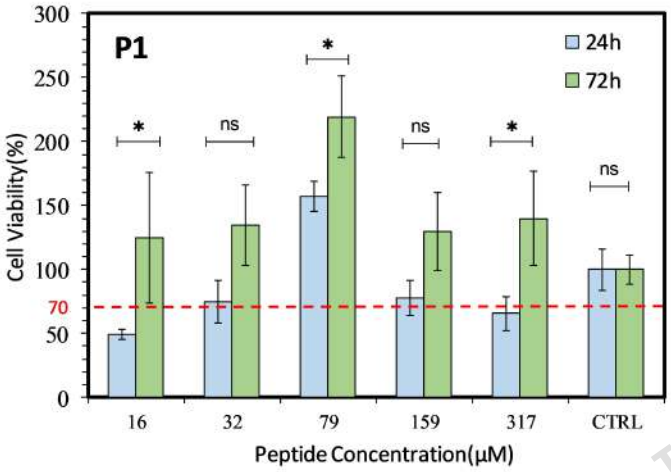

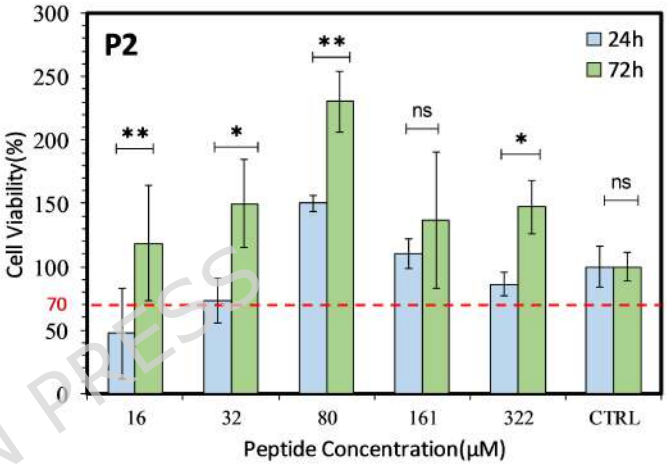

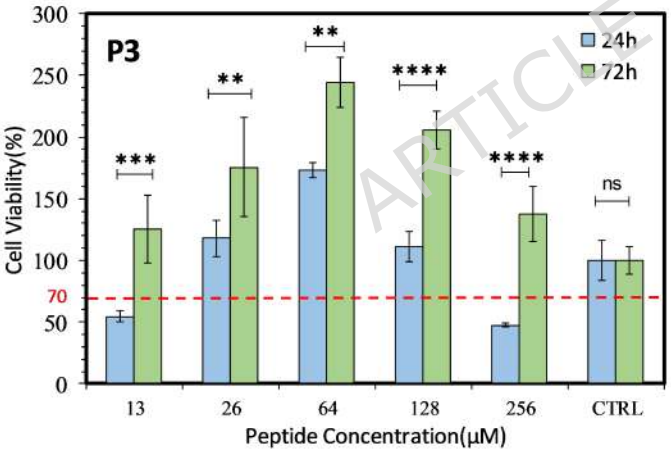

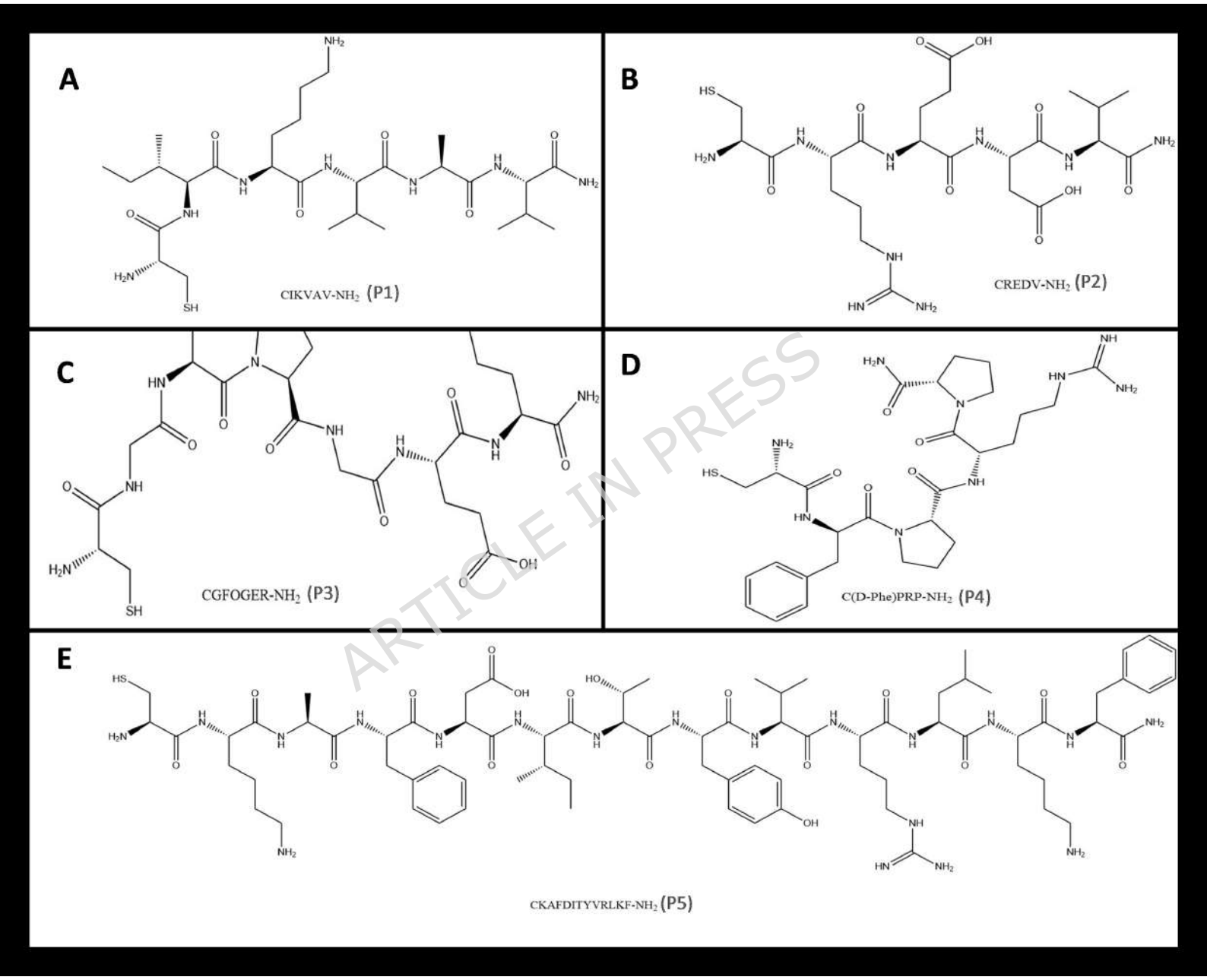

A

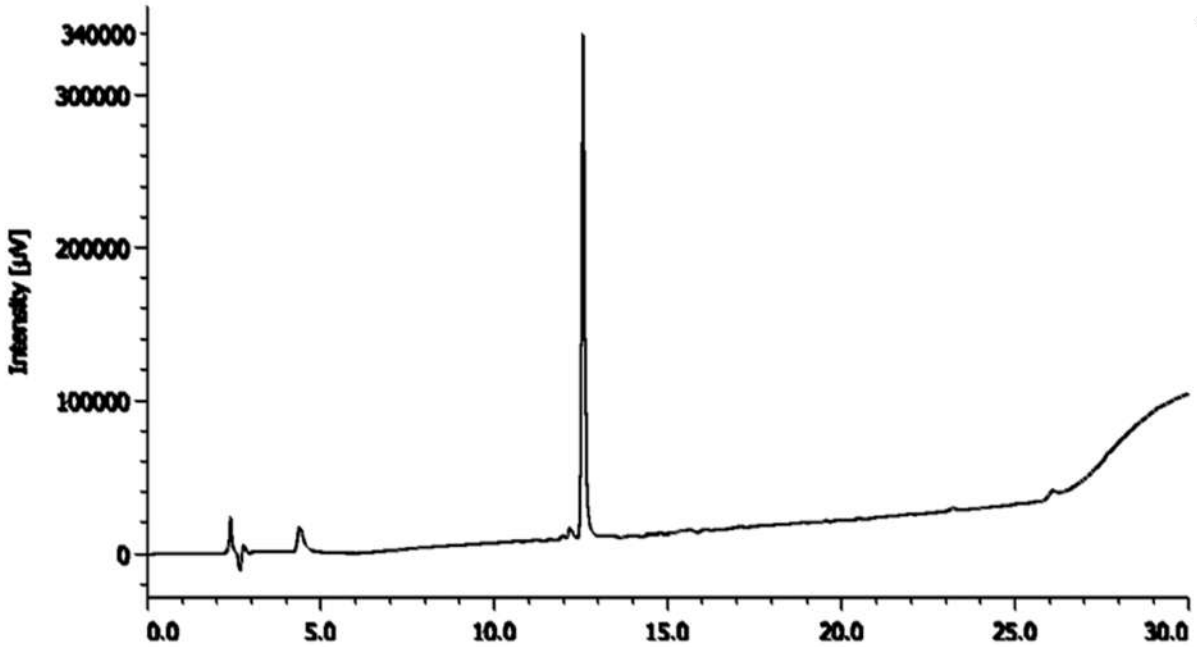

B

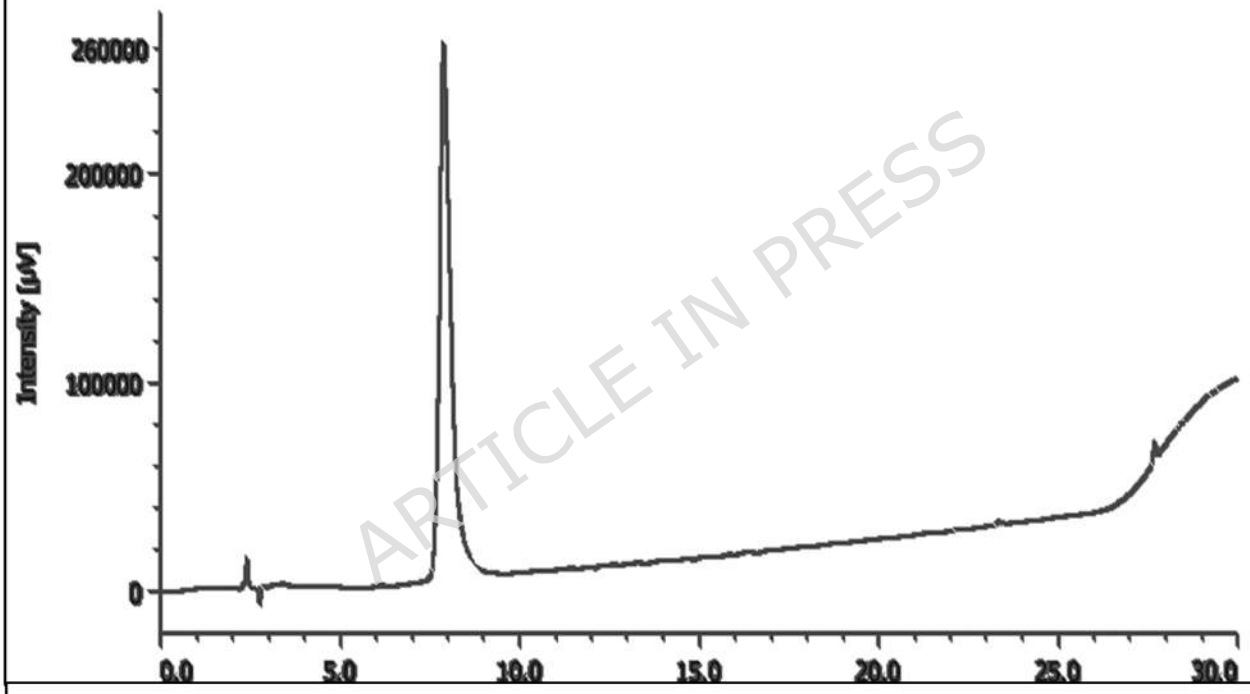

C

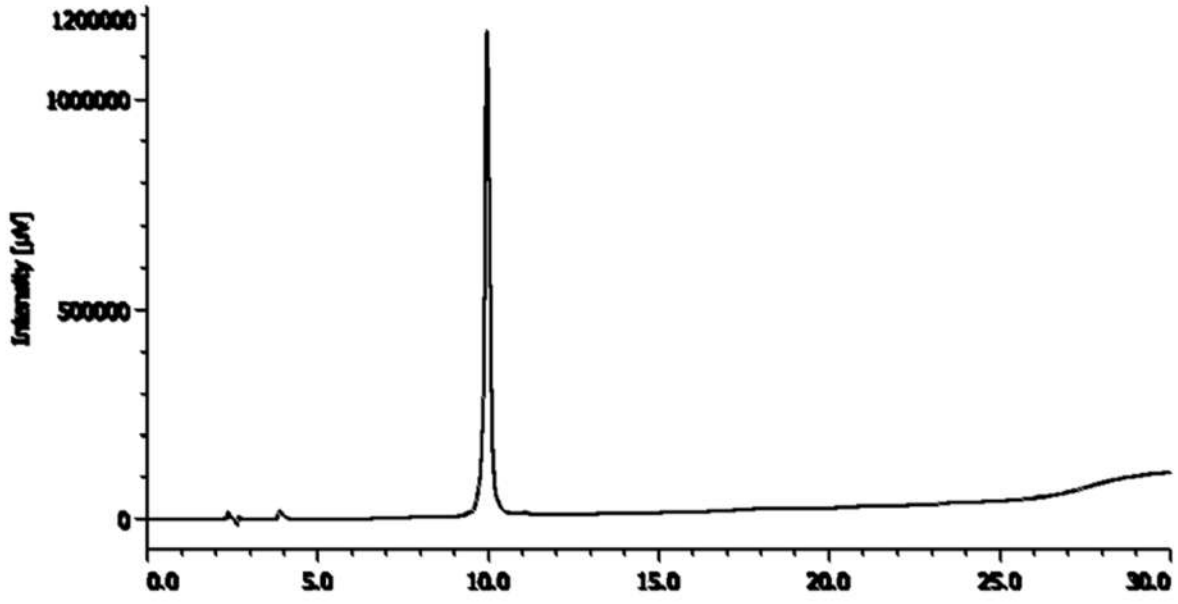

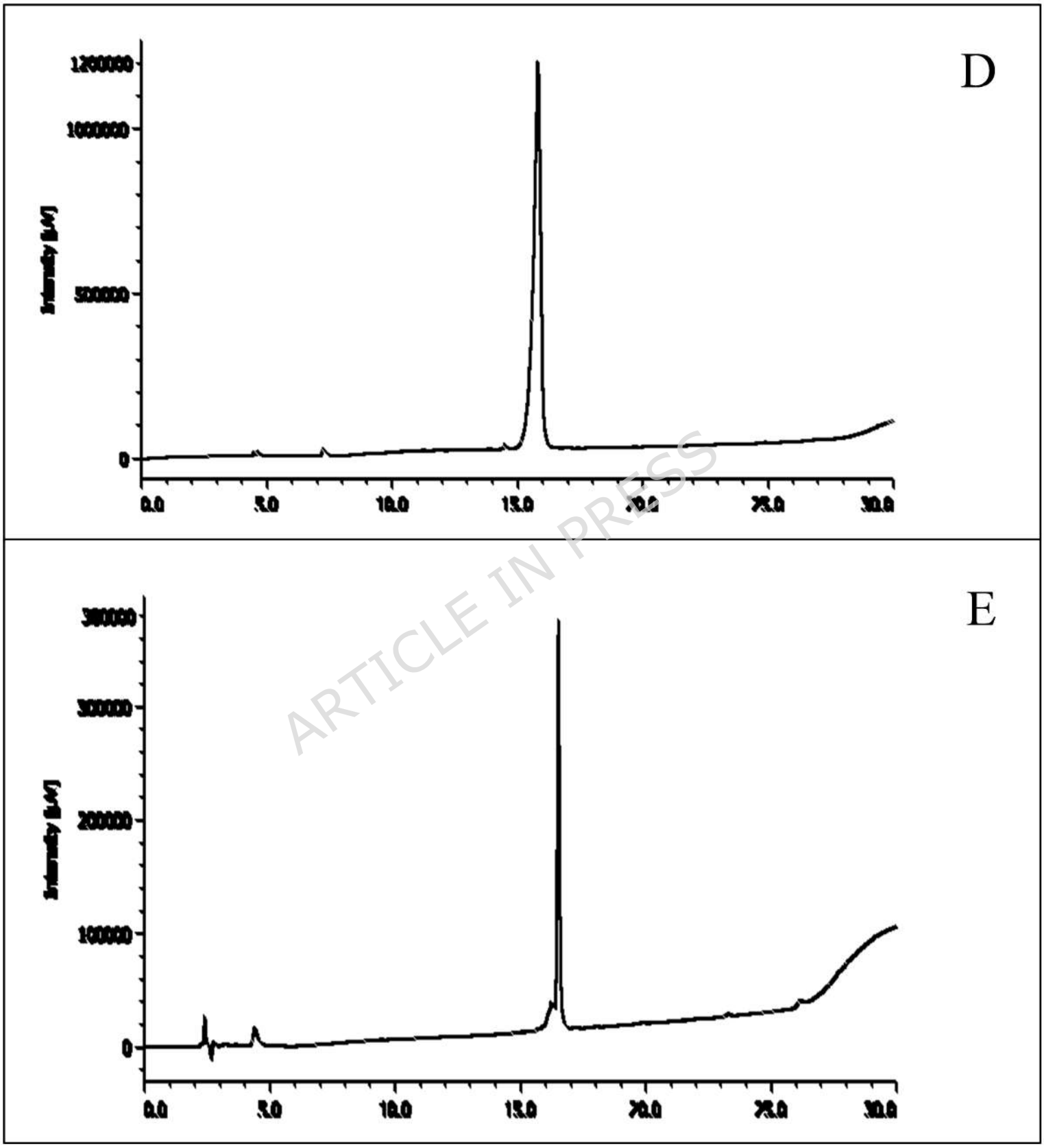

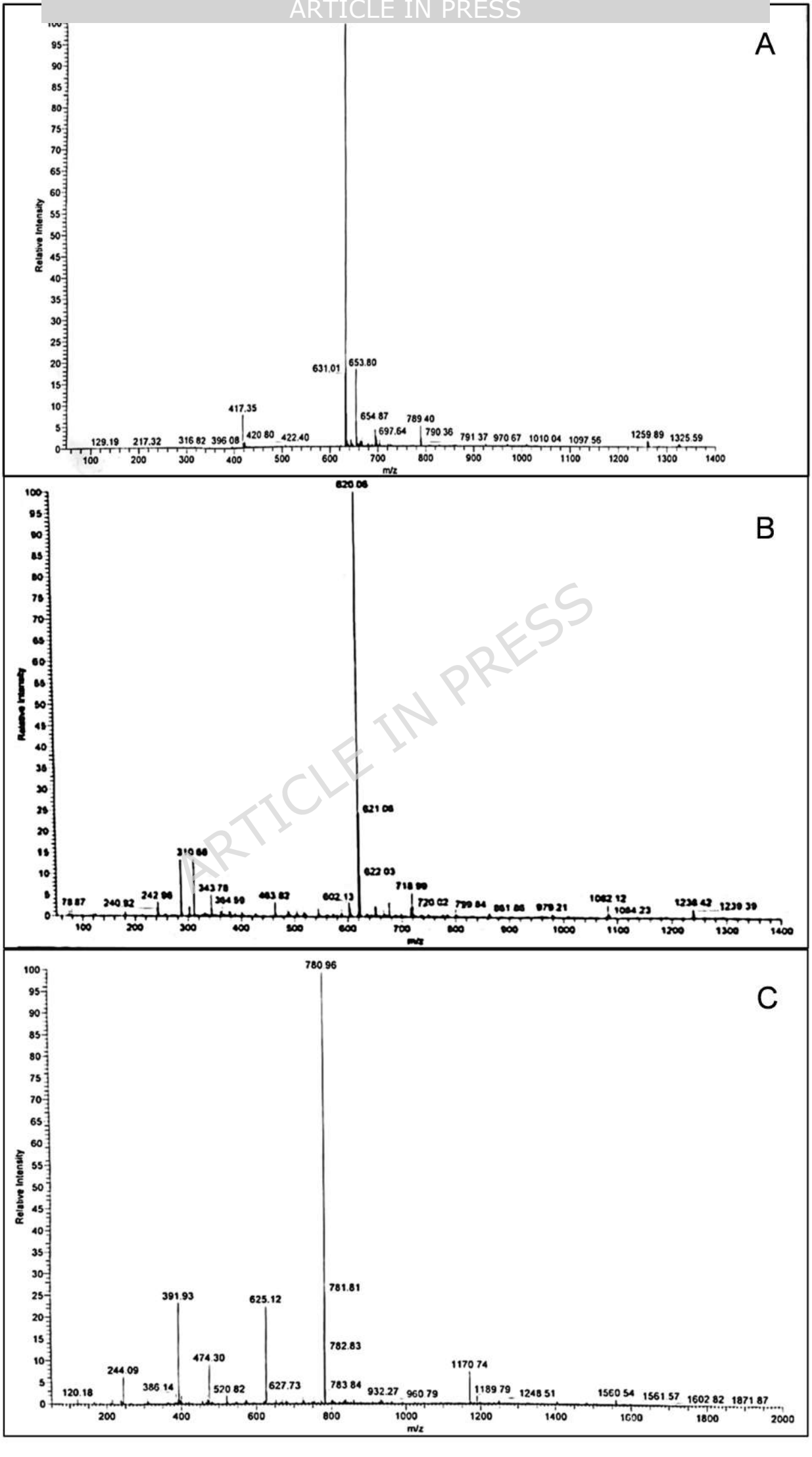

Name	Peptide Sequence	Role	MW exp (g/mol)	MW cld (g/mol)	Purity (%)	Mass (mg)
P1	CIKVAV-NH_2	Promoting endothelial cell proliferation, attachment and angiogenesis	631.79	630.39	94%	41.2mg
P2	CREDV-NH_2	Promoting endothelial cell adhesion	620.06	619.27	100%	58.8 mg
P3	CGFOGER-NH_2	Promoting cell adhesion	780.96	779.34	99%	69.8mg
P4	C(D-Phe)PRP-NH_2	Trombin binding site (Anticoagulation)	619.39	617.31	99%	77.5mg
P5	CKAFDITYVRLKF-NH_2	Pro-angiogenesis	803.05	1601.88	95.3%	27.5mg

UTS (MPa)	Young modulus (MPa)	Yield strength (MPa)	Yield strain (%)	Breaking point (MPa)	Elongation at break (%)
2.9±0.1	54.2±14.6	1.8±0.2	3.1±0.3	2.6±0.1	442.7±48.7

Name	Peptide conjugation (nmol)	Peptide conjugation (μg/mg fibers)	Conjugation efficiency (%)
P1-scaffold	18.9 ± 0.30	6.6 ± 1.1	36.8 ± 6.4
P2-scaffold	15.7 ± 0.58	4.7 ± 1.6	26.8 ± 9.3
P3-scaffold	28.5±1.68	4.6±1.8	21.1± 8.3
P4-scaffold	22.3±6.9	1.8±0.5	10.4±3.1
P5-scaffold	12.9 ± 0.66	9.1 ± 2.7	24.9 ± 11.1